Chemical Geology 351 (2013) 281–298

Contents lists available at SciVerse ScienceDirect

Chemical Geology

journal homepage: www.elsevier.com/locate/chemgeo

Hydrogeochemistry of the Middle Rio Grande aquifer system — Fluid mixing and salinization of the Rio Grande due to fault inputs

Amy J. Williams [a,*], Laura J. Crossey [a], Karl E. Karlstrom [a], Dennis Newell [b], Mark Person [c], Emily Woolsey [c]

[a] University of New Mexico, Department of Earth & Planetary Science, 1 University of New Mexico, Albuquerque, NM 87131, USA
[b] Utah State University, Department of Geology, 4505 Old Main Hill, Logan, UT 84322, USA
[c] New Mexico Institute of Mining and Technology, Department of Earth & Environmental Science, 801 Leroy Place, Socorro, NM 87801, USA

ARTICLE INFO

Article history:
Received 18 October 2012
Received in revised form 11 May 2013
Accepted 17 May 2013
Available online 2 June 2013

Editor: C.M. Koretsky

Keywords:
Groundwater quality
Salinity
Rio Grande
Rio Grande rift
Aqueous geochemistry
Endogenic fluids

ABSTRACT

Deeply-derived fluids influence river and groundwater hydrochemistry at the Socorro "constriction" in the central New Mexico Rio Grande rift. New hydrochemical transects in the Rio Grande rift provide three-dimensional perspectives on sources contributing to surface and groundwaters. In addition to abrupt salinity increases in the Rio Grande, major and trace ion chemistry, $\delta^{18}O$, δD, $\delta^{13}C$, $^{87}Sr/^{86}Sr$, ^{3}H and $^{3}He/^{4}He$ variations in springs and wells across the rift are best explained by mixing of deeply-derived endogenic fluids, containing both mantle and crustal inputs, with shallow groundwater. Endogenic fluids ascend along rift-bounding and intra-rift faults, and can cause increased salinity accompanied by an increase in metals and overall degradation of water quality. Our data reinforce models that attribute a downstream increase in salinity to geological, not agricultural, influences. Hydrochemical mixing of endogenic waters along faults in shallow aquifers has a major influence on groundwater and surface water quality and variability in arid tectonically active regions, with important ramifications for water management.

1. Introduction

The middle Rio Grande basin of the Rio Grande rift in central New Mexico contains a heavily utilized surface–groundwater system that sustains a large population and complex ecosystems. Both high salinity and elevated trace element concentrations have been cited as regionally important concerns that impair water quality (Mills, 2003; Phillips et al., 2003; Newton, 2004; Plummer et al., 2004; Newell et al., 2005; Anning et al., 2007). Identifying and quantifying sources of these constituents remain an ongoing challenge. Sources of both increasing downstream salt levels in the Rio Grande (Ghassemi et al., 1995; Mills, 2003; Hogan et al., 2007) and depth-dependent salinity in the Rio Grande rift alluvial aquifers represent an unresolved combination of influences, such as contributions from rock–water interaction (e.g. dissolution of evaporite deposits), inputs from still deeper saline fluids (Musgrove and Banner, 1993; Newell et al., 2005), and anthropogenic influences such as evapotranspiration from agricultural lands (Wilcox, 1957; Trock et al., 1978).

Here we present new data from a trans-rift cross section of spring and groundwater hydrochemistry in the Sevilleta National Wildlife Refuge (SNWR) and surrounding springs in the central Rio Grande rift, and consider these in the context of published chemistry for the Rio Grande and for the shallow alluvial aquifer system. This region is an ideal location to examine hydrochemical mixing as it contains a rich variety of interacting hydrofacies. Hydrofacies include shallow aquifer systems (as previously described in Plummer et al., 2004), water from various parts of the Rio Grande rift unconfined aquifer hosted in Quaternary/Tertiary fluvial deposits and piedmont deposits, deeper waters from several Paleozoic and Mesozoic aquifers, and hydrothermal and endogenic-influenced waters (Newell et al., 2005).

This general location has also been identified as an important location to examine downstream increases in Rio Grande salinity (Mills, 2003). This paper evaluates alternate, but not mutually exclusive, hypotheses for contributions to the salinity in the Rio Grande: 1) that deeply penetrating faults within the rift provide conduits for deeply derived (endogenic) fluid ascent (Newell et al., 2005; Crossey et al., 2006, 2009), 2) that salts are primarily derived from upwelling sedimentary basin brines (Mills, 2003; Phillips et al., 2003; Hibbs and Merino, 2007; Hogan et al., 2007; Doremus and Lewis, 2008), and 3) anthropogenic salinization (Lippencott, 1939; Wilcox, 1957; vanDenburgh and Feth, 1965; Trock et al., 1978). Endogenic fluids are here defined as deeply sourced fluids from below regional freshwater aquifers, including deep basin brines, with elevated salinity, $[CO_2]$, $^{87}Sr/^{86}Sr$, and mantle-derived helium. The goal of this study is to utilize elemental and isotopic data in a three-dimensional cross section of the rift to investigate the detailed

* Corresponding author at: University of California, Davis, Department of Geology, 1 Shields Avenue, Davis, CA 95616, USA. Tel.: +1 530 754 9982; fax: +1 530 752 0951.
E-mail addresses: amywill@ucdavis.edu (A.J. Williams), lcrossey@unm.edu (L.J. Crossey), kek1@unm.edu (K.E. Karlstrom), dennis.newell@usu.edu (D. Newell), mperson@nmt.edu (M. Person), ewoolsey@nmt.edu (E. Woolsey).

0009-2541/$ – see front matter © 2013 Elsevier B.V. All rights reserved.
http://dx.doi.org/10.1016/j.chemgeo.2013.05.029

geometry and causes of salt and other degradations to the groundwater and surface water systems.

2. Regional background

Continental extensional tectonism began in the Rio Grande rift system 25–30 Ma (Chapin and Cather, 1994) and continues today (Russell and Snelson, 1994; Keller and Baldridge, 1999). Fig. 1 shows the major faults and geologic subdivisions of the central Rio Grande rift. Regionally, the rift is a series of half grabens with alternating asymmetry. In the northern Albuquerque Basin, the dominant fault on the east side of the rift is the west-dipping Sandia–Manzano fault system, whereas in the southern Albuquerque Basin the east-dipping Jeter fault system is dominant. The SNWR is located near the Tijeras accommodation zone, which transfers displacement between these oppositely dipping master fault systems (Fig. 1).

Structural relics of Laramide and earlier events, plus the extensional faults of the Rio Grande rift, create a complex network of faults that now influence groundwater flow (Mailloux et al., 1999; Plummer et al., 2004). Regional structures have been shown to enhance the transport of deep fluids to the surface (Liu et al., 2003; Rzonca and Schulze-Makuch, 2003; Crossey et al., 2006, 2009; Caine and Minor, 2009), and to act as both barriers and conduits for groundwater flow (Mozley and Goodwin, 1995; Rawling et al., 2001). A key region to understand both groundwater and surface water hydrochemistry in the Rio Grande rift is at the SNWR where only limited spring geochemical data were previously available (Spiegel, 1955). This area is located at the intersection of the Albuquerque and Socorro basins at the Socorro "constriction", marking a southward constriction in the Rio Grande rift *sensu stricto*, but a southward expansion from rift structures characterized by alternate asymmetrical half-grabens (Lewis and Baldridge, 1994) to a series of several parallel basins and intra-rift tilted block uplifts of the Basin and Range province (Chapin and Cather, 1994).

Volcanic rocks in the area indicate persistent magmatic/tectonic influences. The Indian Hill volcanics near the San Acacia spring have been dated from 4.9 ± 0.1 Ma (Ar–Ar) (D. Love, Personal communication)

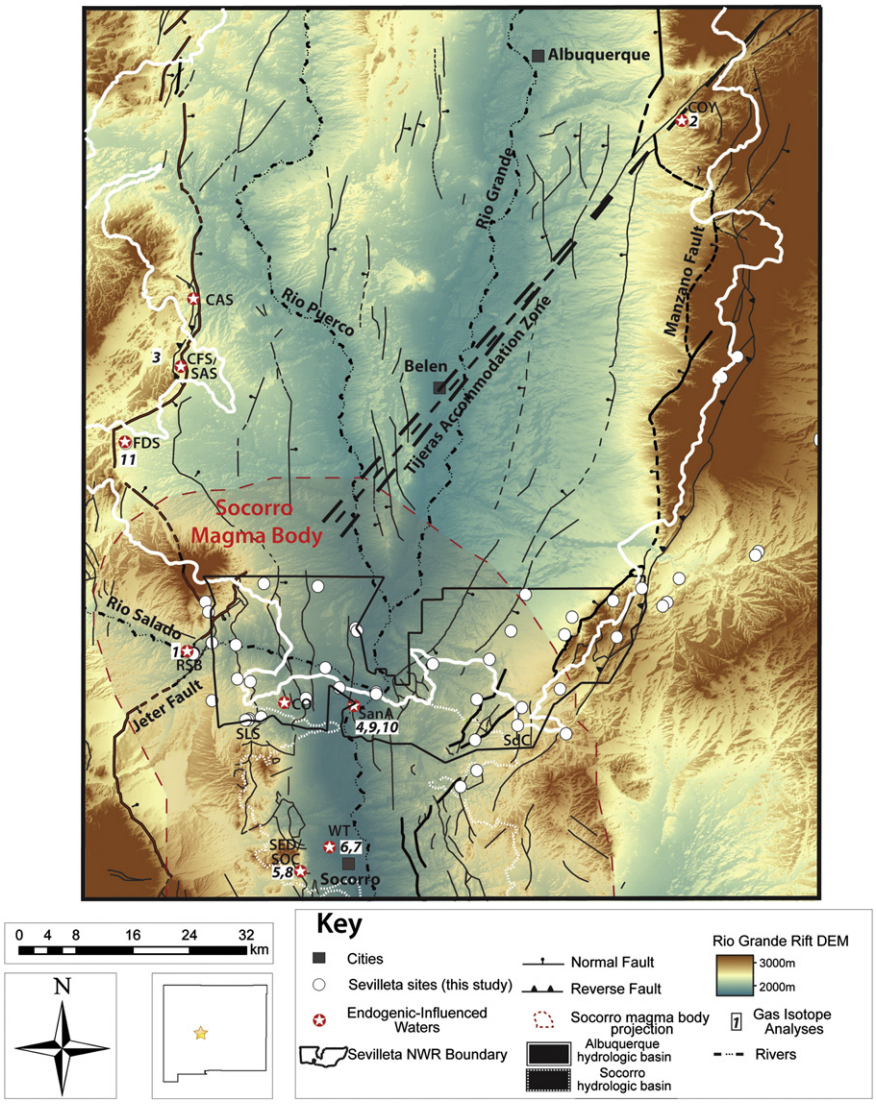

Fig. 1. Digital elevation model of the Rio Grande Rift including the Rio Grande, Rio Salado, and Rio Puerco, Sevilleta NWR, and sample sites from this study. Sevilleta sites identified as hydrochemical facies 1 (endogenically-influenced) are marked with red stars and include Coyote Spring (COY), Carrizo Arroyo spring (CAS), Comanche Fault spring (CFS), Salado Arroyo Spring (SAS), Four Daughters Spring (FDS), Rio Salado Box springs (RSB), Canyon del Ojito spring (CO), San Acacia spring (SanA-C), San Acacia lower pool (SanA-Z), San Acacia well (SAC), New Mexico Tech geothermal well (WT), Sedillo Spring (SED), and Socorro spring (SOC). Sites with measurable mantle helium values are referenced as italicized numbers in white boxes (see Table 1).
Socorro magma body outline modified from Reiter (2009). Tijeras Accommodation Zone modified from May and Russell (1994) and Lewis and Baldridge (1994). Fault outlines modified from Scholle (2003).

and a basalt flow underlying river deposits at San Acacia has been dated from 4.5 ± 0.1 Ma (K–Ar) (Bachman and Mehnert, 1978). These are older than Quaternary eruptions in the Albuquerque/Los Lunas region, which have been dated from 144 ± 4 ka (K–Ar) to 1.25 ± 0.02 Ma (Ar–Ar). Additionally, Quaternary eruptions from the Lucero area have been dated from 278 ± 3 ka (K–Ar) to 800 ± 10 ka (K–Ar) (see citations in Dunbar, 2005), with older basalt flows on the west edge of the rift dating to 4.0 ± 0.3 Ma (Black Mountain, Socorro Canyon) and 3.7 ± 0.4 Ma (Mesa Carrizo along Comanche Fault zone) (both K–Ar) (Bachman and Mehnert, 1978).

There is a strong association of springs and fault systems in the Rio Grande rift. The major springs along the western faults of the study area are Rio Salado Box springs, Four Daughters spring, Comanche fault springs, Salado Arroyo spring, and Carrizo Arroyo springs. Coyote spring is the only major spring along the eastern fault system in this region (Fig. 1). A diffuse accommodation zone (the Tijeras accommodation zone described by May and Russell, 1994; Lewis and Baldridge, 1994) passes roughly through Belen and marks a change in basin asymmetry, but NE-trending surface faults of this system are poorly expressed. Numerous intrabasin faults are N–S normal faults with moderate displacements (Scholle, 2003; De Moor et al., 2005). Another important spring system in the SNWR is San Acacia (SanA). This spring system is located near the center of the rift and the Cliff Fault trace, northeast of the Tertiary age Indian Hill volcanics (Osburn, 1984; Machette et al., 2000).

Fig. 2A shows a three-dimensional block diagram of the study area with the hypothesized flow paths present in the basin fill controlled by mountain-front recharge, deep-seated fault conduits, and potential hydrothermal circulation. In addition to being located at this important structural transition, the SNWR is underlain at 19 km depth by the Socorro magma body and seismic anomaly (Figs. 1 and 2B) and is one of the most neotectonically active regions in New Mexico (Sanford et al., 1977; Larsen et al., 1986; Balch et al., 1997; Fialko and Simons, 2001). Reiter et al. (2010) demonstrated that heat flow near the Socorro magma body is 4.5 to 8 times greater than expected from the imaged sill. They concluded that multiple basaltic intrusions, of which the Socorro magma body is the youngest, are present. The SNWR region is highly faulted and has experienced active magmatism, perhaps through the past several million years (Reiter et al., 2010). Hence, it is an important place to examine possible interactions of tectonic and magmatic features with the hydrologic system.

In terms of surface water, previous geochemical studies have shown a nearly sixty-fold increase in river conductivity (a proxy for salinity), from 90 μS/cm from the headwaters in southern Colorado, to 5300 μS/cm near the Texas/Mexico border during low flow conditions in August (Mills, 2003). River salinity increases markedly as the river passes the San Acacia brine pools (location shown in Fig. 1), with conductivity values on the order of 690–5380 μS/cm. Cl/Br ratios and ^{36}Cl values combined with salinity increases at basin termini indicate that the increase in salinization is due to the geologic addition of saline groundwater and is not primarily from anthropogenic influences (Mills, 2003; Phillips et al., 2003). These authors proposed a model in which sedimentary basin brines upwell at the southern termini of the Albuquerque basin, near San Acacia. Their model (Fig. 3A) depicts long and deep groundwater flow paths along the rift axis where upwelling, driven by hydraulic head, is focused at basin termini. This type of flow could be explained by multi-scale topographically driven groundwater circulation (Toth, 1963). However, topography cannot account for all circulation and high hydraulic head is required to force dense saline waters to upwell. Mapped hydrologic gradients in the Middle Rio Grande basin (Fig. 3B) suggest both E–W flow from recharge in rift flanks uplifts, N–S flow in the basin axis (compatible with Fig. 3A), and local importance of fault conduits (Plummer et al., 2004). Bexfield and Plummer (2003) observed zones of high salinity and arsenic near faults adjacent to city groundwater production wells in the Albuquerque Basin. They attributed the fluid flow along faults to a combination of well pumping and associated declines in the potentiometic surface, and attribute the source of elevated As to be from: 1) a deep source associated with saline brine and 2) siliceous volcanism related to the Valles Caldera.

The model of Phillips et al. (2003) for geologic (non-agricultural) causes of increased river salinity is reinforced in this paper, and we add to this model by exploring possible sources of geological fluid inputs. Fig. 2A shows a hydrogeologic model that emphasizes the importance of faults near rift margins and basin constrictions that may influence the ascent and location of deeply-derived fluid discharge from below the unconfined aquifer. We also contribute to the Phillips et al. (2003) Rio Grande rift upwelling model by considering the potential importance of hydrothermal influences on fluid mixing, explored by Newell (2007). The source of the Na–Cl brine referred to by Phillips et al. (2003) remains an active research topic. We consider possible geologic sources to be: 1) the Yeso Formation and other evaporites in the Paleozoic sedimentary section (although Yeso evaporites contain appreciable gypsum and little halite, whereas the Mills (2003) signal is primarily tracked by Cl and Br), and 2) evolved seawater brines in Mesozoic rocks such as those noted in the San Juan basin (Zhou et al., 2005). A third source is magmatically derived Cl conveyed in magmatic fluids. These fluids may be conveyed upwards to interact with the shallow aquifer system from a fractionally crystallizing Socorro magma body that reached chloride saturation (Anderson, 1974; Schilling et al., 1978; Muramatsu and Wedepohl, 1979; Rowe and Schilling, 1979; Webster and de Vivo, 2002, and references therein).

3. Methods

The SNWR offers an ideal transect to apply multiple tracers to both surface and groundwater in an environment that has been relatively little affected by the anthropogenic influences of grazing and agriculture. To evaluate the presence of deeply sourced fluids into both the surface and groundwater systems of the middle Rio Grande basin, we evaluate major ion and trace element chemistry, stable isotopes of oxygen, hydrogen and carbon ($\delta^{18}O$, δD, $\delta^{13}C$), $^{87}Sr/^{86}Sr$ ratios, tritium (^{3}H) values, $^{3}He/^{4}He$ ratios, and apply geochemical modeling, to develop a hydrogeologic model for understanding fluid flow and water quality. Detailed methods are reported in the Supplementary Material. The natural tracers we use are useful to identify influences of, and mixing between, endogenic waters and meteorically recharged shallow aquifer waters.

The primary data presented is based on a comprehensive study of waters from within and surrounding the SNWR including springs, wells, and surface water samples. Water samples were collected, preserved, and analyzed using standard methods (see Supplementary Material). Springs were sampled at base flow conditions. Wells were pumped of 3 well volumes before collection. Field temperature, pH, and conductivity were recorded (Supplementary Material Table 1).

4. Results and discussion

4.1. Water chemistry and definition of hydrochemical facies

The aqueous chemistry of 83 surface and well waters was determined (Fig. 4). The SNWR waters span the range of water chemistries seen in the Albuquerque Basin (inverted gray triangles, Plummer et al., 2004) such that the SNWR provides a microcosm of Rio Grande rift hydrochemistry. Water compositions are widely variable and cluster into three distinct hydrochemical groups based on major ion data (Supplementary Material Table 1) that also correspond geographically with regions of the SNWR; a Na–Cl group, a mixed ion–HCO_3 group, and a Ca–SO_4 group (Fig. 4). These groups are combined with field parameters and local geology and structure to define three hydrochemical facies. Hydrochemical facies 1 waters have a Na–Cl composition (Fig. 4 — closed stars, circles, inverted triangles) and include springs on large rift-bounding faults, wells along the Rio Salado, and intra-rift fault

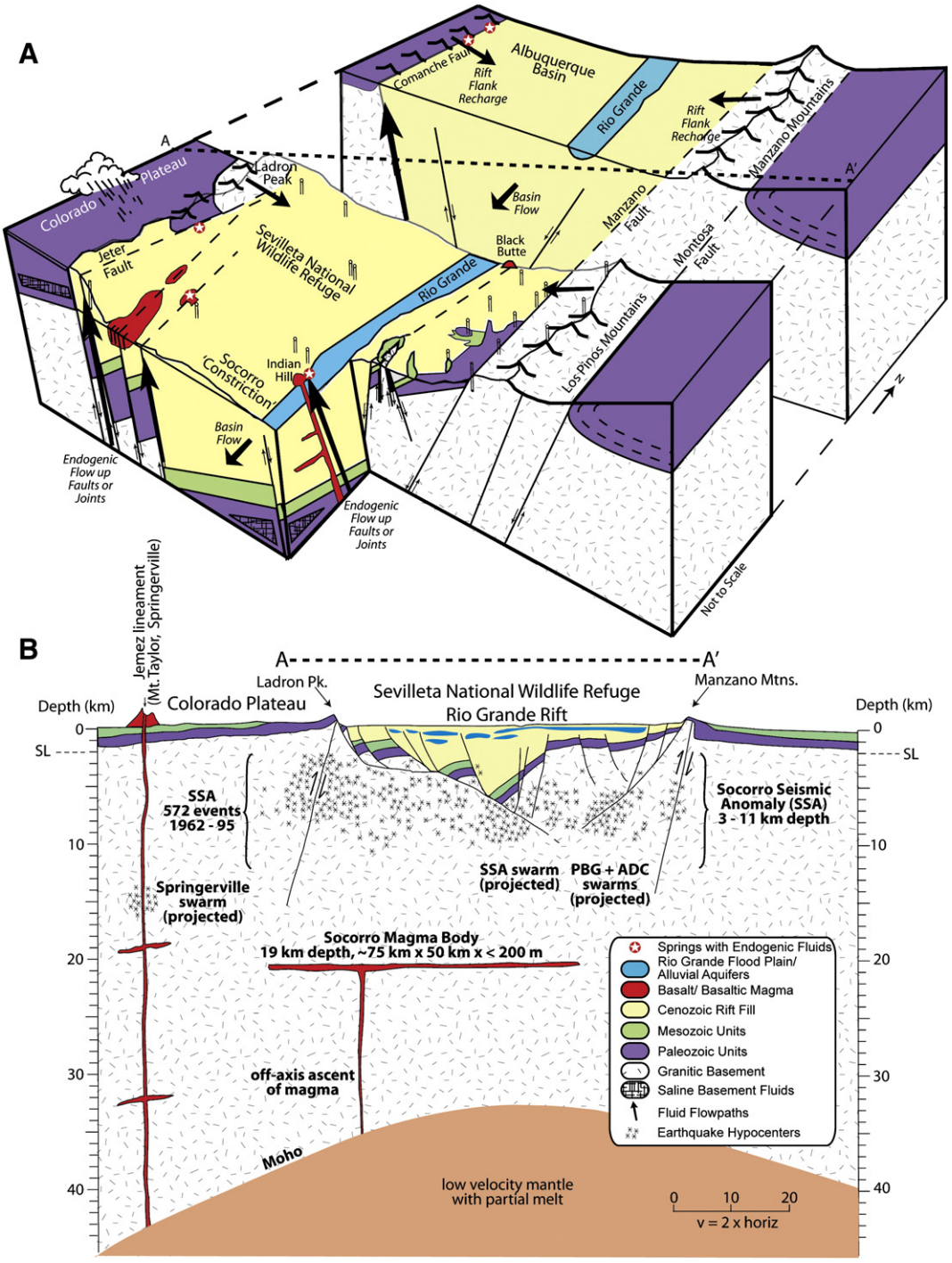

Fig. 2. A. Three-dimensional schematic block diagram of the middle Rio Grande rift with hypothesized flowpaths for basin flow, rift flank recharge, and endogenic flow up faults (arrows). Saline point sources are identified by starred symbols. B. Cross section interpreted from the CoCorp seismic line showing the Rio Grande rift, Colorado Plateau, Socorro Seismic Anomaly, and Socorro magma body. The Socorro magma body is hypothesized to contribute to the anomalously high seismicity of the Socorro Seismic Anomaly and to contribute magmatic mantle-derived helium and CO_2 to springs of the region.

controlled springs near San Acacia. These waters exhibit elevated temperatures, conductivity, TDS, and trace metals (Table Supplementary Material 1 and 3), and elevated pCO_2. Hydrochemical facies 2 contains a mixed cation–HCO_3 composition (Fig. 4 — closed triangles) and are found in springs on the southwest side of the SNWR, which is dominated by Tertiary volcanics and Quaternary/Tertiary rift fill. Hydrochemical facies 3 contains Ca–SO_4-rich waters (Fig. 4 — closed diamonds) that are found primarily on the southeast side of the SNWR, an area dominated

Fig. 3. A. Hydrogeologic cross section parallel to the Rio Grande showing postulated flowpaths of upwelling brines at basin termini. This paper adds a modified geologic model involving faults near basin termini and a magmatic/hydrothermal mechanism for upwelling of endogenic fluids that entrain deep basin brines and also mix in the shallow aquifer system. B. Water levels and equipotential surface in the Middle Rio Grande basin. Matrix flow into and through the basin is assumed to be perpendicular to equipotential contours (arrows). Fluid fast-pathways may exist parallel to N–S faults.
Panel A is modified from Mills (2003). Panel B is modified from Plummer et al. (2004).

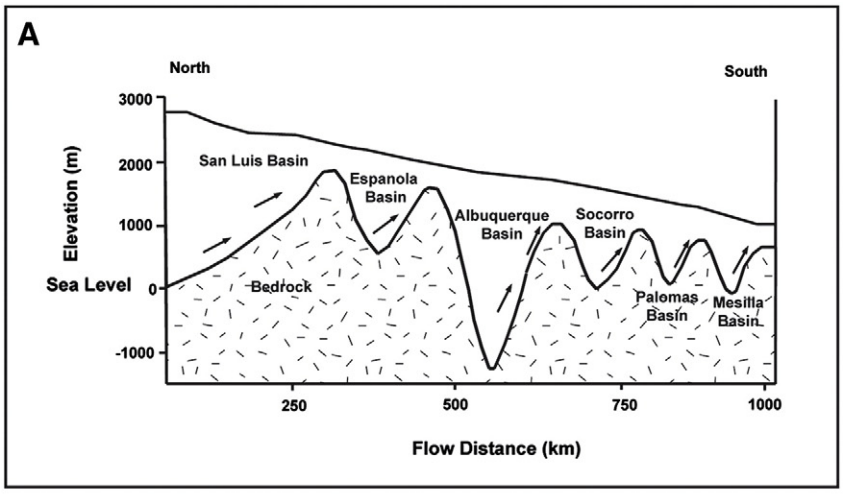
A
North
South
Elevation (m)
3000
2000
1000
0
-1000
Sea Level
San Luis Basin
Espanola Basin
Albuquerque Basin
Socorro Basin
Palomas Basin
Mesilla Basin
Bedrock
250
500
750
1000
Flow Distance (km)

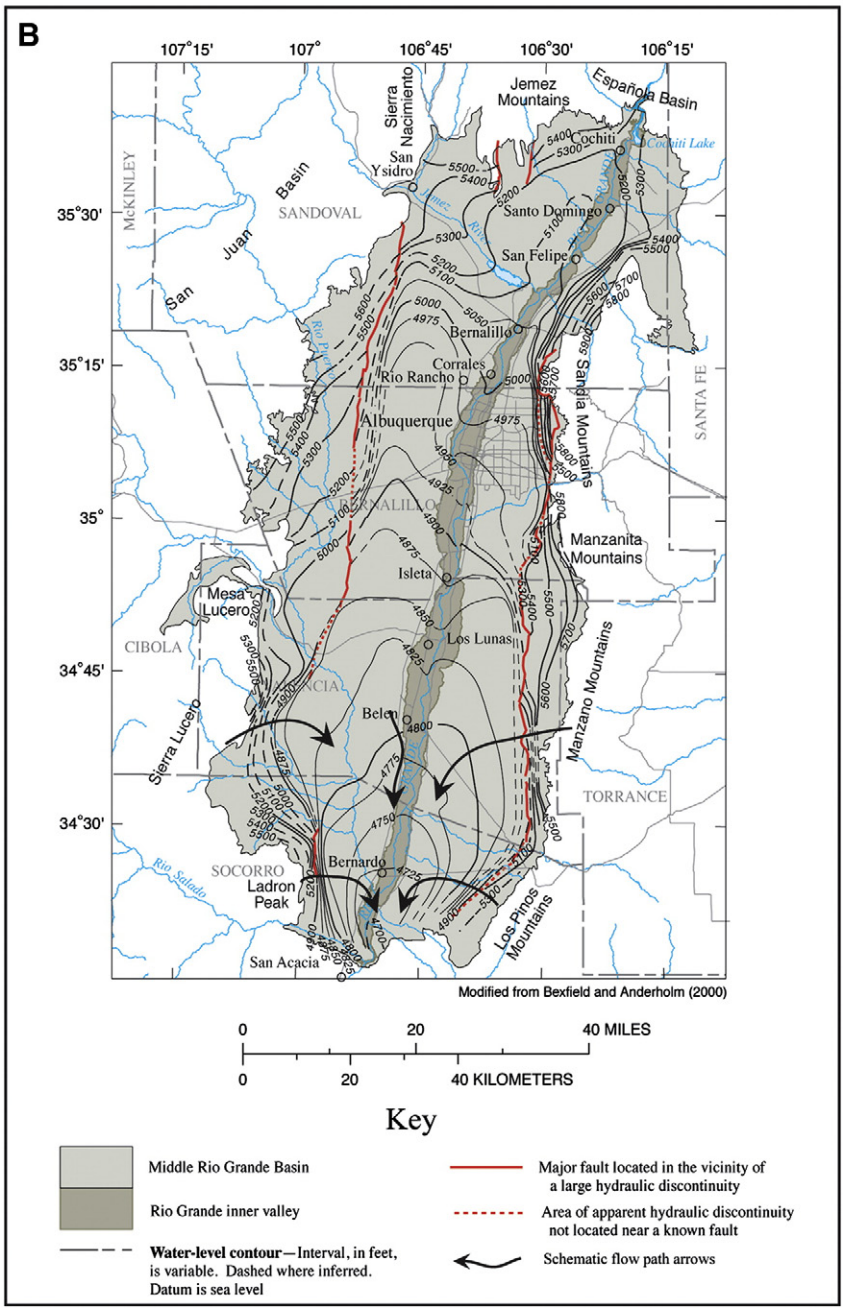
B
107°15'
107°
106°45'
106°30'
106°15'
35°30'
35°15'
35°
34°45'
34°30'
Sierra Nacimiento
Jemez Mountains
Española Basin
Cochiti Lake
San Ysidro
Santo Domingo
San Felipe
Bernalillo
Corrales
Rio Rancho
Albuquerque
Sandia Mountains
Manzanita Mountains
Isleta
Mesa Lucero
Los Lunas
Manzano Mountains
Belen
Sierra Lucero
Bernardo
Ladron Peak
San Acacia
Los Pinos Mountains
McKINLEY
SANDOVAL
SANTA FE
CIBOLA
TORRANCE
SOCORRO
San Juan Basin
Rio Puerco
Rio Salado
Modified from Bexfield and Anderholm (2000)
0 20 40 MILES
0 20 40 KILOMETERS
Key
Middle Rio Grande Basin
Rio Grande inner valley
Water-level contour—Interval, in feet, is variable. Dashed where inferred. Datum is sea level
Major fault located in the vicinity of a large hydraulic discontinuity
Area of apparent hydraulic discontinuity not located near a known fault
Schematic flow path arrows

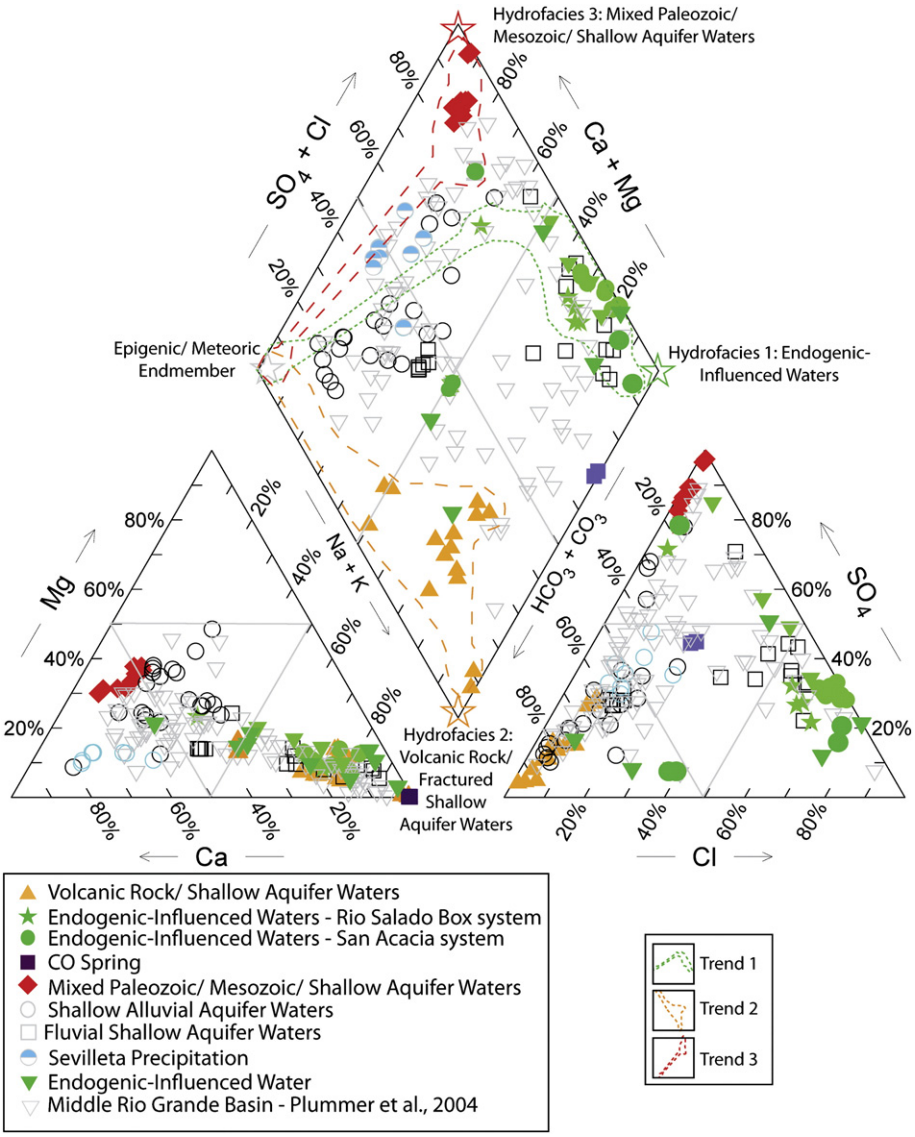

Fig. 4. Piper diagram of SNWR waters showing hydrochemical mixing trends between 3 different hydrochemical facies with an epigenic/meteoric endmember (at left of parallelogram). Distinct mixing trends define three geographically distinct hydrochemical groups: Hydrochemical facies 1 is Na–Cl waters from the west and mid-regions (includes Rio Salado Box system — stars and San Acacia system — closed circles), Hydrochemical facies 2 includes mixed cation–HCO_3 waters from the southwestern region (open triangles), and Hydrochemical facies 3 is Ca–SO_4 waters from the southeastern region (diamonds). In the background are water chemistries from the Albuquerque Basin showing that water chemistry variation and mixing trends in the SNWR is a microcosm of the entire Albuquerque Basin.
From Plummer et al. (2004).

by Permian and Pennsylvanian-aged sedimentary units such as the gypsum-bearing Yeso Formation. These waters exhibit elevated TDS and are found on a series of small NE–SW trending faults. Another group in Fig. 4 has a mixed cation–anion composition (open circles) consistent with local precipitation chemistry (semi-closed circles) and is found in the northern region of the SNWR. The mixed ion waters are sampled from wells in the Santa Fe Group aquifer across the northern extent of the SNWR. A group of mixed cation–Cl waters (open squares) are from the Rio Grande and Rio Salado waters and adjacent wells, have a similar geochemistry to shallow alluvial aquifer waters but a distinctly higher [Cl] signature. Lastly, the closed square symbols in Fig. 4 delineate one spring found along a fault in volcanic rock that exhibits a unique Na + K/mixed anion chemistry. All of these hydrochemical facies exhibit mixing between dilute meteoric values (star at left of parallelogram) with proposed near-endmember compositions (other three parallelogram corners).

The distribution of water chemistries across the SNWR, as newly resolved here, is shown in Fig. 5. The new data reported here are geographically consistent with chemistries reported in Plummer et al. (2004) and Roybal (1991), and extend the characterization of these hydrochemical facies further south (Fig. 5).

Cl/Br mass ratios were calculated from major ion chemistry to evaluate salinity and the influence of evapotranspiration in the hydrochemical facies (Fig. 6). Hydrochemical facies 1 has a range from 72 (SOC) to 2181 (RSB12), with most ratios above 1200. Hydrochemical facies 2 has a range from 20 (SC1) to 190 (SC2) and hydrochemical facies 3 has a range of 14 (SdC3) to 172 (GW) (Supplementary Material Table 2). Kendrick et al (2012) found that mantle Cl/Br ratios isolated from back arc basins and seamounts range from 205 to 459, whereas Davis et al. (1998) reported ratios of 1000 to 10,000 in waters influenced by halite dissolution. The hydrochemical facies 1 Cl/Br ratios may contain a combination of halite dissolution-influenced waters, deeply derived fluids, and meteoric water to achieve the Cl/Br ratio of the Rio Salado Box springs and San Acacia system. Evaporative concentration can mostly account for the subsequent increase in [Cl] to the San Acacia lower pool (Fig. 6). Once halite saturation occurs, further evapotranspiration leads to a

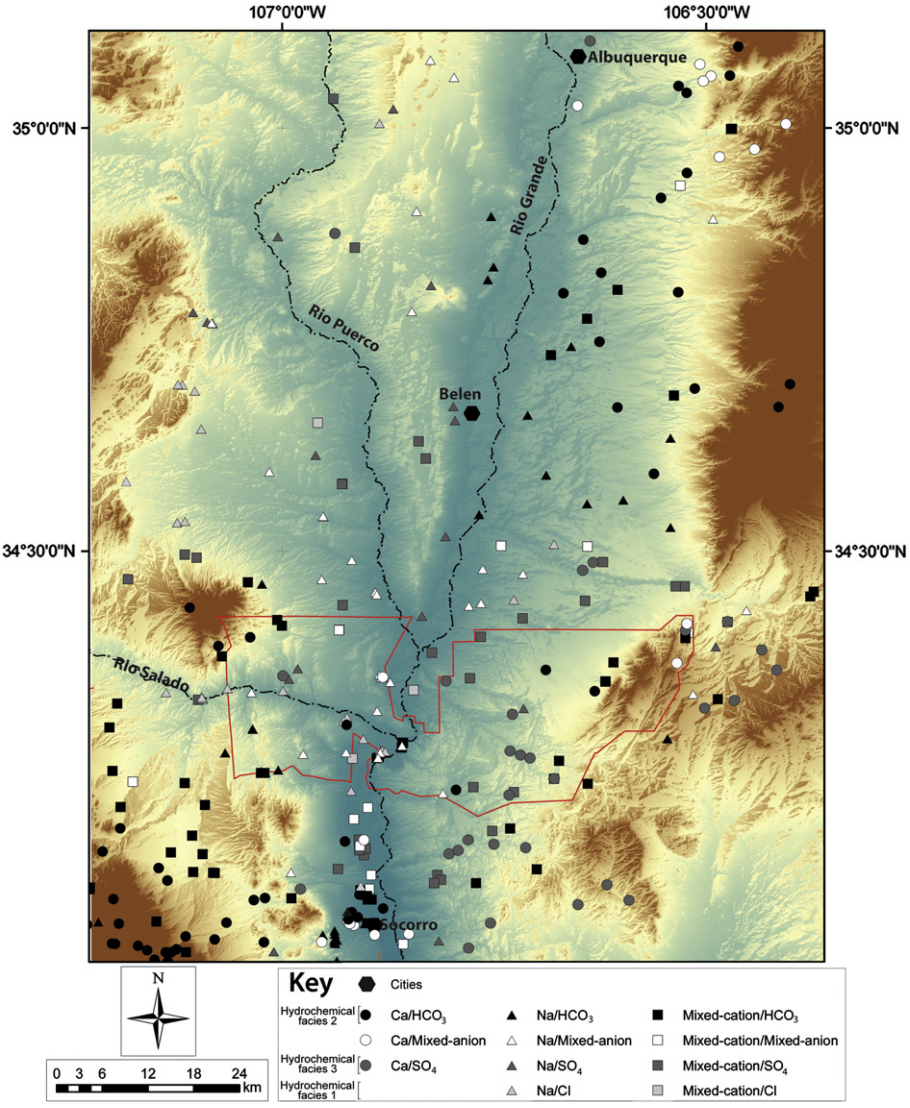

Fig. 5. Water types of groundwater samples in the Middle Rio Grande basin (water types based on the Piper diagram from Fig. 4). Samples are from Plummer et al. (2004), Roybal (1991), and this study.

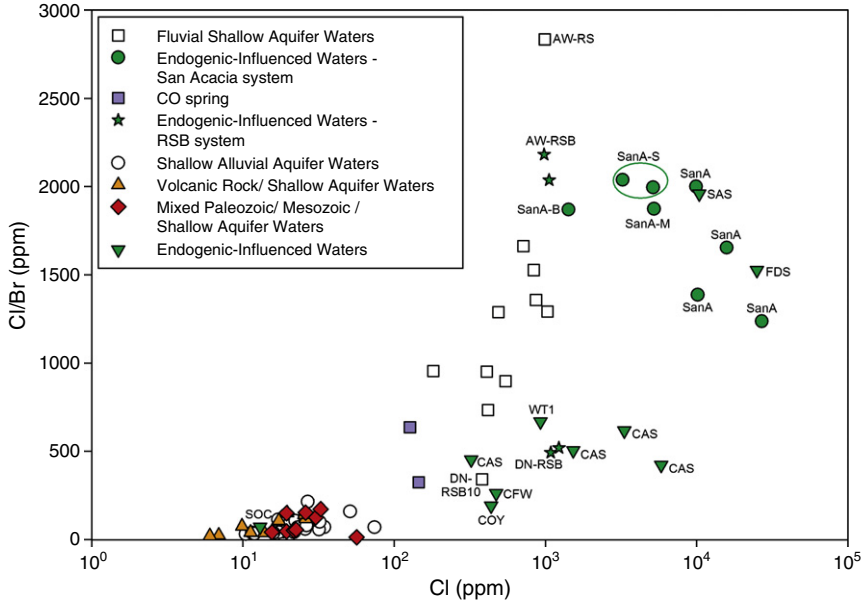

Fig. 6. Cl/Br ratio versus [Cl] for SNWR waters. Geographically controlled hydrochemical facies are shown in the same colors as Fig. 4.

progressive decrease in Cl/Br (Land and Prezbindowski, 1981; Fontes and Matray, 1993; Bottomley et al., 1994).

Of relevance for water quality, the highest trace element concentrations (Supplementary Material Table 3) are reported from hydrochemical facies 1 waters. Of these, the Rio Salado Box and San Acacia systems consistently had the highest trace element concentrations of all waters (Fig. 7). Ba, Li, and B are consistently elevated in CO_2-charged springs (Newell et al., 2005; Crossey et al., 2006) and are often also associated with higher salt content. Thus, the deeply derived endmembers degrade water quality in ways similar to what is observed in geothermal systems (Plummer et al., 2004; Crossey et al., 2009), where water quality degradation can be considered roughly proportional to volumes of contributed deeply derived fluids. The high trace element concentrations measured in the Rio Salado Box and San Acacia systems suggest that these two Cl-dominated endmembers contain some component of geothermal/deeply derived fluids to attain the high values detected.

4.2. Isotopic analyses ($\delta^{18}O$, δD, $\delta^{13}C$, $^{87}Sr/^{86}Sr$, ^{3}H)

Oxygen and hydrogen stable isotopic compositions ($\delta^{18}O$ and δD) ranged from 8.3‰ to −11.9‰ and 1.6‰ to −92.5‰ (VSMOW), respectively. Fourteen samples analyzed for $\delta^{13}C$ (from DIC) ranged from −0.8‰ to −16.5‰ (VPDB) (Supplementary Material Table 3). For comparison, brachiopods, whole rock, and cement samples from the upper Pennsylvanian Madera Limestone have an average $\delta^{13}C = 0.57‰$ (Brand, 2004), marine limestones generally have $\delta^{13}C = 0$ to 2‰ (Sharp, 2007), mantle gases have $\delta^{13}C = -6 \pm 2‰$ (Sano and Marty, 1995), and soil gas has strongly negative values as low as $\delta^{13}C = -28‰$ (Sano and Marty, 1995). Hydrochemical facies 1 waters had a $\delta^{13}C$ range from −9.5‰ to 0.8‰, while $\delta^{18}O$ and δD ranged from −3.2‰ to 8.3‰ and 1.6‰ to −67.8‰, respectively. Hydrochemical facies 2 waters had a $\delta^{13}C$ range from −16.5‰ to −4.8‰, while $\delta^{18}O$ and δD ranged from −6.5‰ to −8.9‰ and −53.0‰ to −67.2‰, respectively. Hydrochemical facies 3 waters had a $\delta^{13}C$ range from −8.3‰ to −1.6‰, while $\delta^{18}O$ and δD ranged from −5.1‰ to −8.5‰ and −45.2‰ to −59.4‰, respectively. In contrast, the Rio Grande isotopic composition in the study area ranges from $\delta D = -80.0$ to −85.0‰ and $\delta^{18}O = -10.2$ to −11.1‰ (Mills, 2003), while regional precipitation isotopic values from this study range from $\delta D = -38.4$ to −51.5‰ and $\delta^{18}O = -5.9$ to −8.1‰, Trends in $\delta^{18}O$, δD, and $\delta^{13}C$ are discussed below.

$^{87}Sr/^{86}Sr$ ratios ranged from 0.7090 (SdC1) to 0.7152 (DN-RSB12) (Supplementary Material Table 3). Hydrochemical facies 1 waters ranged from 0.7097 to 0.7152. The San Acacia samples are similar to the range for Paleozoic marine carbonate values (0.7060–0.7100; Burke et al., 1982), and for the middle to upper Pennsylvanian Madera Formation specifically (0.7066–0.7118; Mukhopadhyay and Brookins, 1976). Similar $^{87}Sr/^{86}Sr$ values were determined for the Rio Grande headwaters (0.7096; Hogan et al., 2007). Higher values of 0.7147 and 0.7152 in the Canyon del Ojito Spring and Rio Salado Box spring, respectively, suggest water–rock interaction during crustal circulation in more radiogenic granitic basement, which can have values ranging from 0.7350 to 0.7480 (Crossey et al., 2006). Mixing models (Crossey et al., 2006) suggest that the values of 0.7152 could be achieved with about 1% of high $^{87}Sr/^{86}Sr$ (e.g. 0.7480) fluid volume mixed with meteoric water (e.g. 0.7090). All other samples, including hydrochemical facies 2 and 3 had a limited range of 0.7090 to 0.7100 with the exception of SLS1 (0.7127). The importance of the $^{87}Sr/^{86}Sr$ data in the SNWR is that it provides evidence for mixing of fluids that have interacted with granitic basement and indicates that low volume of deeply derived inputs into groundwaters may have significant geochemical effects on the surface water system. An influx of more radiogenic $^{87}Sr/^{86}Sr$ spring water to the Rio Grande can explain a downstream increase in Rio Grande $^{87}Sr/^{86}Sr$ ratios from San Marcial, NM to El Paso, TX, which show markedly higher downstream values (0.7112; Moore et al., 2008) relative to the headwaters (0.7096; Hogan et al., 2007). This is similar to the downstream increase in $^{87}Sr/^{86}Sr$ ratios in the Colorado River from 0.7100 to 0.7110 between Lake Powell and Lake Mead (Patchett and Spencer, 2001), attributed to inputs from endogenic fluid-sourced tributary springs (Crossey et al., 2006, 2009). Albuquerque Basin deep saline groundwater show a range of values (0.7093–0.7118; Plummer et al., 2004), that likely also reflects mixing with a radiogenic source.

Tritium analyses yielded values ranging from 0.7 TU (CO) to 4.7 TU (SanA lower brine pool) (Supplementary Material Table 3) for select SNWR waters. A common interpretation is that waters with <0.8 TU recharged before 1952, 0.8–4 TU indicate a mix of recent water and pre-1952 recharge, and 5–15 TU indicate recharge from the last 5–10 years (Hurst, 2003). As such, the tritium values presented here can be considered a general indicator of mixing between younger recharge and some component of older waters. Precipitation in Albuquerque averaged 9.1 TU in 1997 (young recharge) and the Rio Grande in

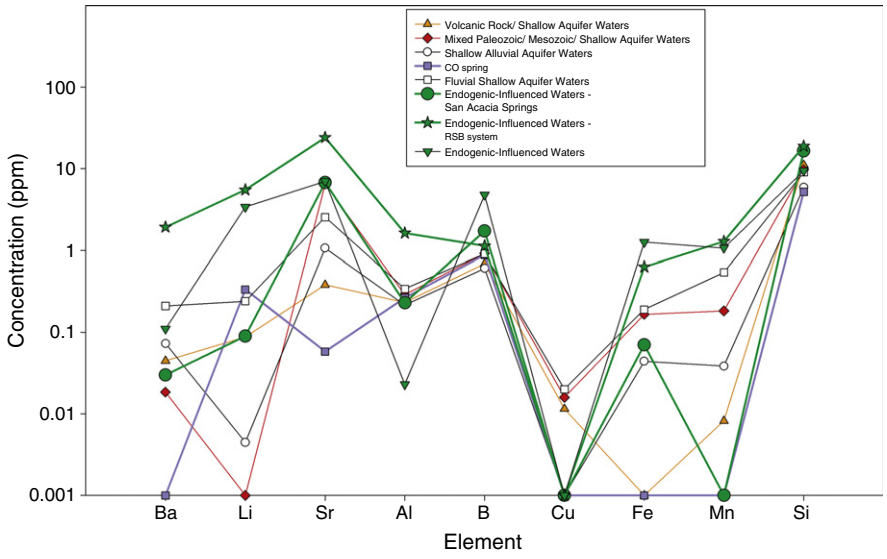

Fig. 7. Averaged trace element spidergram of the major hydrochemical facies. Endogenically-influenced waters have been divided into San Acacia spring waters (closed circle), Rio Salado Box springs 11 and 12 (star) and the remaining endogenically-influenced waters (closed downward triangle). Hydrochemical facies 1 (endogenic-influenced waters) consistently have the highest concentrations of trace elements of all waters sampled.

Albuquerque averaged 9.2 TU from 1997 to 1998 (Plummer et al., 2004). Although age is not well constrained, the older waters found in the middle Rio Grande rift may be up to tens of thousands of years old (Plummer et al., 2004). Our data are interpreted to reflect mixing of variable proportions of older (tritium-dead) fluids with young meteoric inputs. Canyon del Ojito spring (0.7 TU) and two wells (FWS, 0.6 TU and TUW, 0.7 TU) demonstrate a strong pre-1952 recharge signal, suggesting a greater addition of tritium-dead water or a long recharge flowpath. Other waters exhibit mixtures of more pre-1952 recharge relative to recent recharge (NW, 0.9 TU and GW, 1.1 TU). SLS1 (2.7 TU) and SdC1 (3.8 TU) exhibit mixing of more recent recharge relative to pre-1952 recharge, and the San Acacia lower pool tritium value (4.7 TU) indicates that a majority of the water is derived from recent recharge, indicative of the mixture of precipitation and San Acacia spring input.

4.3. Trace gases and helium isotope data

Helium isotopes provide the best evidence for the presence of a component of mantle-derived volatiles in the hydrologic system and here we report gas chemistry data for selected springs. The ^{3}He isotope was acquired during Earth's accretion (Clarke et al., 1969), while ^{4}He is the radiogenic decay product of U and Th. Helium isotope ratios (R) are referenced to air (R_A) which has a $^3He/^4He = 1.4 \times 10^{-6}$ (Graham, 2002). The modern $^3He/^4He$ ratio at mid-ocean ridges is 8 ± 1 R_A (Graham, 2002), while regions isolated from asthenospheric flux such as the Canadian Shield have $^3He/^4He$ ratios for groundwaters of ~0.02 R_A (Andrews, 1985). Ratios of $R_C/R_A > 0.1$, where R_C reflects the air-corrected helium isotope ratio (Welhan et al., 1988) and hence reflects non-air-like gases, are interpreted to contain a significant mantle-derived He component (Craig et al., 1978; Kennedy et al., 1985, 1987, 2002; Ballentine and Burnard, 2002; Ballentine et al., 2002).

The $^3He/^4He$ ratio of some Albuquerque Basin waters provides evidence for the presence of mantle-derived volatiles in the groundwater system (Table 1). The highest air-corrected values (R_C/R_A) are 1.907 R_A from the New Mexico Tech geothermal well, which corresponds to about 24% mantle-derived helium (assuming a mantle end-member of 8 R_A). The suspected endogenically-influenced springs in the SNWR also show mantle helium contributions; Rio Salado Box springs has a value of 0.370 R_A (~5% mantle helium) and San Acacia spring has a value of 0.357 R_A (~4% mantle helium), while the San Acacia well has a value of 0.830 R_A. Along eastern rift-bounding faults, Coyote Fault well and Coyote Springs have R_C/R_A values of 0.596 to 0.870 R_A (7.5–11% mantle helium), respectively. Along the western rift bounding faults, Four Daughters Spring has an R_C/R_A value of 0.587 R_A (7% mantle helium). All the springs and groundwaters analyzed for $^3He/^4He$ show values of > 0.1 R_A and are interpreted to reflect measurable inputs of mantle helium into the aquifer system.

$^3He/^4He$ ratios measured in waters from this region reflects a complex set of variables including long flow paths and fluid mixing. We assume that mantle volatiles are MORB-like (~8 R_A) because of seismic evidence for asthenospheric upwelling. However, input from the lithospheric mantle (~4 R_A; Reed and Graham, 1996) is also likely. At lithospheric scale, the volatile ascension pathways likely involve the same paths as the basaltic magmatism of the Socorro magma body and ^{4}He is progressively added during ascent through radiogenic isotope-bearing crust which lowers the $^3He/^4He$ ratio (Kennedy et al., 1997). Upper crustal volatile pathways seem to be concentrated along both rift-bounding faults and intra-rift faults as shown by the locations of the high $^3He/^4He$ ratio springs along such faults. We assume that ascent of a mixed CO_2/H_2O fluid is associated with the intense shallow microseismicity of the Socorro seismic anomaly (depicted in Fig. 2B; Sanford et al., 1977; Larsen et al., 1986; Balch et al., 1997; Fialko and Simons, 2001), which has had 572 events (generally <3 R magnitude) in a 33 year period (Reiter, 2005). Hence, this is an especially likely region to convey endogenic fluid up faults and into the near surface hydrologic system.

Sources of helium to these waters include mantle/crustal contributions and tritiogenic addition from mixing with post-atomic bomb peak recharge (post 1963). Mixing analyses have shown that, although a few endogenically-influenced waters (SAW, SAC, SOC, EDD, FDS) have ^{3}He concentrations that could contain a significant fraction of tritiogenic He, most endogenically-influenced waters (SAS, COY, CFW, RSB, CFW duplicate, WT1, and WT2) contain orders of magnitude greater amounts of ^{3}He than can be accounted for by $^3He_{tritiogenic}$ contributions alone (maximum 1.7E−13 cm^3 STP/g in 1963) (Supplementary Material Fig. 3). Indeed, it is possible that none of the ^{3}He measured be derived from ^{3}H if a mixing component is younger than ~1980. To achieve the ^{3}He values measured in the low [^{3}He] waters would require mixing with a specific pulse of 1960 to 1980 water that only impacts select waters. This mixing analysis supports our interpretation of a mixture of crustal and mantle sources traced by the $^3He/^4He$ ratio.

4.4. Interpretation of hydrochemical facies and water sources

The series of tracers discussed above consistently demonstrate the presence of three geochemically distinct hydrochemical groups based on major ion, trace element, trace gases, stable and radiogenic isotopic data. The mixing trends identified in Fig. 4 suggest mixing between hydrochemical facies 1, 2 and 3 and a meteoric endmember. These mixing trends seem to be unique to their local chemical inputs and each has a separate hypothesized flowpath, as described below.

Hydrochemical facies 1 waters are Na–Cl waters that correlate with elevated temperatures, conductivity, TDS, [Cl], $^{87}Sr/^{86}Sr$ ratios, trace metals, mantle helium signatures, and include CO_2-exsolving springs on large rift-bounding faults, wells along the Rio Salado, and intra-rift fault springs near San Acacia. The mixing trend is interpreted to reflect mixing of endogenically-influenced fault-related fluids (possibly including hydrothermal and magmatically influenced fluids) with meteoric inputs.

Hydrochemical facies 2 waters are SNWR southwest region-specific mixed cation–HCO_3 waters that correlate with low temperature, conductivity, TDS, [Cl], Cl/Br, $^{87}Sr/^{86}Sr$ ratios and low $\delta^{13}C$ composition and are interpreted as meteoric water interacting with local volcanic units (e.g. rhyolite of the La Jencia tuff; Chamberlain et al., 2004), and/or volcaniclastic rift fill sediments to form volcanic rock/fractured shallow aquifer waters.

Hydrochemical facies 3 waters are SNWR southeast region-specific Ca–SO_4 waters (located along a series of small NE–SW trending faults) that correlate with low temperature, [Cl], Cl/Br, and $^{87}Sr/^{86}Sr$ ratios, and elevated conductivity, TDS, and [SO_4]. These are interpreted to be mixed Paleozoic/Mesozoic/shallow aquifer waters formed from leaching of the Permian Abo and gypsum-rich Yeso Formations and subsequently mixed with meteoric water.

The other groups of geochemically similar waters identified in Fig. 8 can be labeled based on their collective geochemistry and geologic relationships. The mixed ion waters (open circles), collected from shallow wells up to 91 m deep in the Santa Fe Group sediments, are interpreted as shallow alluvial aquifer waters. Shallow alluvial aquifer waters are close to the meteoric endmember in Fig. 4 and exhibit subtle differences from local precipitation in both major ion geochemistry and $\delta^{18}O/\delta D$. The mixed cation–Cl waters (open squares) are interpreted as fluvial shallow aquifer waters, as the samples are from the Rio Grande and Rio Salado waters and adjacent wells, have a similar geochemistry to shallow alluvial aquifer waters but with a distinctly higher [Cl] signature, and a lack of endogenic-influenced water components. The hydrochemical group and geographic location of samples is summarized in Fig. 8.

4.5. PHREEQc modeling of CO_2 saturation

Helium is often carried to the surface by CO_2-rich fluids (Dunai and Porcelli, 2002). To elucidate the source of these CO_2-rich fluids

Table 1
Compilation of new (bolded) and published helium isotopic data from the Middle Rio Grande area, central New Mexico.

1	2	3	4	5	6	7	8	9	10	11
Abbreviations	Sample ID	Site name	Latitude	Longitude	T (°C)	pH	TDS (ppm)	Alk (mg/l)	R/RA	X
1. COY	**LC06NM-COY**	**Coyote spring**	**34.99858**	**−106.47126**	**5.9**	**11**	**2030**	**1269**	**0.910**	**3.10**
2. CFW	**CTF-MW2**	**Coyote fault well**	**35.29162**	**−106.89399**	**14.85**	**5.44**	**2010**	**1843**	**0.621**	**1351.00**
3. CFW	**CTF-MW2 duplicate**	**Coyote fault well-duplicate**	**35.29162**	**−106.89399**	**14.85**	**5.44**	**2010**	**1843**	**0.597**	**287.00**
4. EDD	**DN04-MDO-6**	**Eddelman spring**	**34.78589**	**−106.40411**	**17.1**	**6.9**	**3660**	**553.6**	**0.880**	**4.09**
6. SAS	DN04-SS-20	Salado Arroyo Spring	34.69717	−106.12283	19.2	6.5	16950	2040	0.641	11.37
7. FDS	**LC09-4daughters-1**	**Four Daughters spring**	**34.59329**	**−107.19149**	**11.8**	**7.04**	**50700**	**744.4**	**0.875**	**1.50**
8. RSB	**DN04-RSB12**	**Rio Salado Box spring**	**34.32758**	**−107.09457**	**21.9**	**5.73**	**2885**	**403.2**	**0.370**	**89.90**
9. SAC	**LC10-SanA-C-1**	**San Acacia spring**	**34.26384**	**−106.87876**	**23.3**	**6.72**	**3500**	**219.66**	**0.357**	**7.40**
10. SAW	**DN05-SAC-1**	**San Acacia Well**	**34.27861**	**−106.90445**	**nr**	**nr**	**nr**	**nr**	**0.830**	**6.02**
11. SAP	**AW082209-SanA-Z**	**San Acacia puddle**	**34.26361**	**−106.88416**	**18.8**	**6.76**	**3030**	**nr**	**0.945**	**nr**
12. WT1	**LC10NMWTwell-1**	**New Mexico Tech geothermal well-1**	**34.07323**	**−106.94501**	**25.9**	**6.89**	**1995**	**349**	**1.406**	**3105.00**
13. WT2	**LC10NMWTwell-2[a]**	**New Mexico Tech geothermal well-2**	**34.07323**	**−106.94501**	**25.9**	**6.89**	**1995**	**349**	**1.907**	**1413.00**
14. SED	nr	Sedillo spring	34.03700	−106.93800	nr	nr	nr	nr	nr	nr
15. SOC	**LC10NMSoccorro sp**	**Socorro spring**	**34.04141**	**−106.93507**	**32**	**7.52**	**188**	**159**	**0.401**	**4.14**

Key to column numbers: (bold — new data from this study):

1. Abbreviations used in various plots and figures.
4–5. UTM coordinates using NAD 83.
6–8. Field parameters measured with Oakton Series probe.
9. Alkalinity (as bicarbonate).
10. R/RA = $^3He/^4He$ of sample / $^3He/^4He$ of air (1.4×10^{-6}).
11. X = air contamination factor = (measured He/Ne) / (He/Ne in air) × Bunsen solubility coefficient of Ne to He at 15 °C (method of Hilton, 1996).
12. Rc/RA = corrected $^3He/^4He$; for Hilton lab samples: RC/RA = ((R/RA * X) − 1) / (X − 1)) corrects for air saturated water contamination; for Poreda lab samples, RC/RA correction described in Welhan et al. (1988) and includes both air and ASW contamination.
13. Helium concentration in cm^3 STP/g H_2O.
14. Total CO_2 g/cm^3.
15–16. Measured values; note that $CO_2/^3He$ for mantle is 2×10^9.
17. C isotopes derived from water as extracted from copper tubes.
18. % of CO_2 derived from C_{carb}, C_{endo} and C_{org} based on major element water chemistry.
19. % of ^3He derived from MORB-like mantle sources.
20. References: Hilton = Scripps lab; Poreda = Rochester Lab, see Supplemental Materials for methods; Newell et al., 2005 = reported in Newell et al. (2005).aWT2 CO_2 sources calculated from WT1 water chemistry.

in groundwaters and evaluate CO_2 saturation, we used the geochemical modeling program PHREEQc (Parkhurst and Appelo, 1999) (Supplementary Material Table 4). Groundwater equilibrated with atmospheric CO_2 should have a log $P_{CO_2} < -3.5$, while infiltrated waters with added soil-derived CO_2 (e.g., from microbial respiration) may have log $P_{CO_2} \sim -2.0$ and can reach up to an order of magnitude higher (Drever, 1997; Crossey et al., 2006). In contrast, the log P_{CO_2} values of SNWR spring waters can have much higher P_{CO_2}. Six samples (the San Acacia pools, Canyon del Ojito spring, and the Silver Creek seeps) have log P_{CO_2} values <−3.5, interpreted to be equilibrated with air. These results are expected, as these samples were collected from low flow springs and, in the case of the San Acacia pools, large standing bodies of water. 53 samples (including samples from all hydrochemical facies) have log P_{CO_2} values between −3.5 and −2, compatible with soil-influenced CO_2 values. 17 samples (also represented by all hydrochemical facies, and including the Rio Salado Box springs, San Acacia spring, Cibola spring, and some well waters) have log P_{CO_2} values >−2, with ranges from −1.6 to −1.4, interpreted to be waters that equilibrated in the subsurface at elevated P_{CO_2} that was orders of magnitude higher than atmospheric values of log $P_{CO_2} = -3.5$.

Using PHREEQc, saturation indices were computed for the minerals calcite, dolomite, gypsum, and halite, represented as logIAP/K_{sp} (Supplementary Material Table 4). These were chosen as the likely minerals affecting water chemistry through solution/precipitation reactions based on geologic mapping efforts. Most waters in the SNWR are supersaturated with respect to calcite, although several waters with elevated P_{CO_2} levels are not. Interestingly, sample AW-RSB12, which emanates from limestone, has an elevated log $P_{CO_2} = -1.4$ but is undersaturated with respect to calcite. This suggests that the Rio Salado Box waters have a deep source of CO_2 (compatible with the He data), and that they pass through the limestone too quickly to allow equilibration by dissolution. In addition, these waters need to degas to reach saturation. This is observed at many travertine-depositing springs where travertine precipitates some distance downstream as water degases and pH climbs (Crossey et al., 2009).

4.6. Sources of CO_2

To deconvolve the various sources of CO_2, we used the approach of Fontes and Garnier (1979) as applied by Chiodini et al. (2000, 2004) and modified by Crossey et al. (2009). We used major ion water chemistry and a simple geochemical model to estimate the amount of CO_2 contributed by the dissolution of carbonates (C_{carb}), as illustrated by the following equation: "external CO_2" + H_2O + $(Ca_x,Mg_{1-x})CO_3 \rightarrow XCa + (1-X)Mg + 2HCO_3$. The "external CO_2" (also referred to as "excess CO_2"; Earman et al., 2005), is the CO_2 that cannot be accounted for by dissolution of carbonate rock (including cements as well as carbonates in and below the aquifer). The $C_{external}$ can then be further resolved based upon $\delta^{13}C$ values into CO_2 components derived from organic matter/biological sources ($C_{organic}$) versus those derived from the crust and mantle ($C_{endogenic}$).

In this approach, we compute: 1) the total DIC using PHREEQc (Parkhurst and Appelo, 1999) as the measured alkalinity plus carbon contributed by carbonic acid, 2) the amount of Ca in the fluid due to gypsum dissolution = SO_4 content (all units in mol/L) which is insignificant, 3) the amount of HCO_3 contributed from Ca/Mg-carbonate dissolution is $C_{carb} = [Ca + Mg - SO_4]$, and 4) the amount of carbon contributed from external sources is then $C_{external} = DIC - C_{carb}$, in mol of carbon/L. This approach assumes that Ca + Mg contributions from water–rock interaction with silicates are volumetrically minor. For example, some cations could be contributed from ion exchange during water–rock interactions, but this process is generally considered to be of second-order importance as shown by a strong overall correlation between lower ionic strength (Ca + Mg) and (SO_4 + HCO_3) in

12	13	14	15	16	17	18			19	20
RC/RA	[He]c (cm^3 STP/g H_2O)	Total CO_2 (cm^3/g)	Methane (cm^3/g)	$CO_2/^3He$ (cm^3 STP/g H_2O)	$\delta^{13}C$ (‰) (from CO_2)	CO_2 sources			%MORB	Reference
						$\%C_{carb}$	$\%C_{endo}$	$\%C_{org}$	^3He	
0.870	**3.42E−07**	**nr**	**nr**	**2.25E+12**	**−1.3**	**nr**	**nr**	**nr**	**10.9**	**Hilton**
0.621	**1.75E−05**	**2.15E−01**	**nr**	**1.41E+10**	**−2.2**	**nr**	**nr**	**nr**	**7.8**	**Poreda**
0.596	**3.98E−05**	**1.95E+00**	**nr**	**5.87E+09**	**nr**	**nr**	**nr**	**nr**	**7.5**	**Poreda**
0.850	**1.60E−08**	**8.60E−01**	**1.85E−03**	**4.50E+13**	**nr**	**nr**	**nr**	**nr**	**10.6**	**Hilton**
0.610	2.19E−07	9.24E−01	nr	5.10E+12	−1.0	0.5	68.5	31.1	7.6	Newell et al., 2005
0.587	**1.60E−08**	**1.,25E−01**	**1.33E−03**	**3.24E+13**	**−4.0**	**nr**	**nr**	**nr**	**7.3**	**Poreda**
0.370	**4.65E−05**	**6.40E−02**	**6.70E−05**	**8.57E+09**	**−4.3**	**nr**	**nr**	**nr**	**4.6**	**Hilton**
0.256	**1.62E−07**	**2.71E−02**	**nr**	**5.49E+11**	**−8.2**	**18.4**	**17.1**	**64.54**	**3.2**	**Poreda**
0.800	**1.30E−07**	**nr**	**nr**	**1.62E+12**	**−13.7**	**37.8**	**0.0**	**62.17**	**10.0**	**Hilton**
nr	**5.77E−08**	**2.45E−01**	**2.58E−03**	**3.23E+12**	**−10.7**	**nr**	**nr**	**nr**	**0.0**	**Poreda**
1.406	**1.28E−04**	**1.90E−02**	**nr**	**7.54E+07**	**−3.0**	**nr**	**nr**	**nr**	**17.6**	**Poreda**
1.907	**1.02E−04**	**1.51E−02**	**nr**	**5.54E+07**	**−5.9**	**6.5**	**9.9**	**83.63**	**23.8**	**Poreda**
0.400	nr	nr	nr	nr	nr	nr	nr	nr	5.0	Newell et al., 2005
0.202	**9.20E−08**	**1.01E−01**	**nr**	**1.96E+12**	**−3.6**	**nr**	**nr**	**nr**	**2.5**	**Poreda**

many datasets (Barrett and Pearl, 1978; Crossey et al., 2009) (Supplementary Material Fig. 1). Also, Na and Cl balance each other over a wide range of salinities, which supports the assumption that dissolution of carbonate and sulfate minerals contributes most of the Ca and Mg in the system (Supplementary Material Fig. 2).

However, in some systems, the dissolution of other evaporite minerals (magnesite, trona, burkeite; Earman et al., 2005) also contributes a significant portion of the Ca and Mg to the system, as we postulate for Hydrochemical facies 3 in the southeastern SNWR. In this case, steps 1 and 2 are computed again, but Mg is included in the evaporite correction as opposed to being added to the C_{carb} calculation. The amount of carbon contributed from external sources is again $C_{external} = DIC - C_{carb}$, in mol of carbon/L. Using only the gypsum correction, calculated percents of C_{org}, C_{carb} and C_{endo} are all >100. In these situations, this evaporite correction was used instead. Supplementary Material Table 4 shows the waters that are variably saturated with respect to gypsum and calcite. Thus, the combination of these two treatments applied to different waters depending on computed saturation indices is a modification that improves the method and maximizes C_{carb} and hence provides a minimum estimate of the parameter of greater interest, $C_{external}$.

To deconvolve $C_{external}$ into its $C_{organic}$ and $C_{endogenic}$ components, for each individual sample, we first calculate the $\delta^{13}C$ of the $C_{external}$ using the following equation:

$$\left(\delta^{13}C_{external} \times C_{external}\right) = \left(\delta^{13}C_{DIC} \times DIC\right) - \left(\delta^{13}C_{carb} \times C_{carb}\right).$$

We set the $\delta^{13}C_{carb} = +1‰$. Depending on the region, researchers have used average values of 0‰ (Sharp, 2007; Karlstrom et al., 2013) to +2‰ (Chiodini et al., 2000; Crossey et al., 2009). The C_{ext} calculation is not particularly sensitive to which value is used. Therefore we set $\delta^{13}C_{carb} = +1‰$ instead of the average upper Pennsylvanian Madera limestone value of $\delta^{13}C_{carb} = +0.57‰$ (Brand, 2004).

$C_{external}$ is made up of both biological ($C_{organic}$) and deep ($C_{endogenic}$) sources. In Fig. 9, we plot the calculated $\delta^{13}C_{external}$ for each spring relative to its $C_{external}$. We illustrate the binary nature of $C_{external}$ by superimposing evolution curves (Faure, 1998) representing the addition of an endogenic end member ($\delta^{13}C_{endogenic} = -6‰$ and $C_{external} = \gg 0.06$ mol/L) to an organic carbon end member ($\delta^{13}C_{organic} = -28‰$ and variable $C_{external}$ values of 0.0001–0.004 mol/L). $C_{organic}$ is here considered to be CO_2 from microbial respiration as well as oxidation of sedimentary organic carbon. Chiodini et al. (2000) and Crossey et al. (2009) used empirically derived $\delta^{13}C_{endogenic}$ endmember values of −1‰ to −4.5‰. Our endmember isotopic compositions were selected on the basis of examining the extremes of our own data, with the knowledge that $\delta^{13}C_{organic}$ in vegetated areas has a range of values of −15‰ to −30‰ (Deines et al., 1974; Robinson and Scrimgeour, 1995). Our data largely fall within the evolution curves. We note that our endmember $\delta^{13}C_{endogenic} = -6‰$ also falls within the range of MORB $\delta^{13}C$ of $-6 \pm 2‰$ (Sano and Marty, 1995).

Fig. 9 reinforces the interpretation that certain springs are point sources for CO_2 input from endogenic fluids. Degassing prior to sampling may have driven $\delta^{13}CO_2$ to more positive values (e.g. Newell, 2007; Crossey et al., 2009) for the two RSB samples that plot above the mixing curve. Regardless, it is clear that the high $^3He/^4He$ springs of San Acacia and Rio Salado Box, previously identified as near-endmembers within Hydrochemical facies 1 in this system (Fig. 4), also plot closer to the endogenic CO_2 endmember. The San Acacia and Rio Salado Box springs are similar to other Rio Grande rift CO_2-rich springs, with >75% of the CO_2 derived from deep sources (Newell et al., 2005). Conversely, springs with <50% external carbon are dominated by $\delta^{13}C_{external} < -17‰$ (Fig. 9), compatible with organic carbon-influenced $\delta^{13}C$ values and water chemistries that are dominantly meteoric.

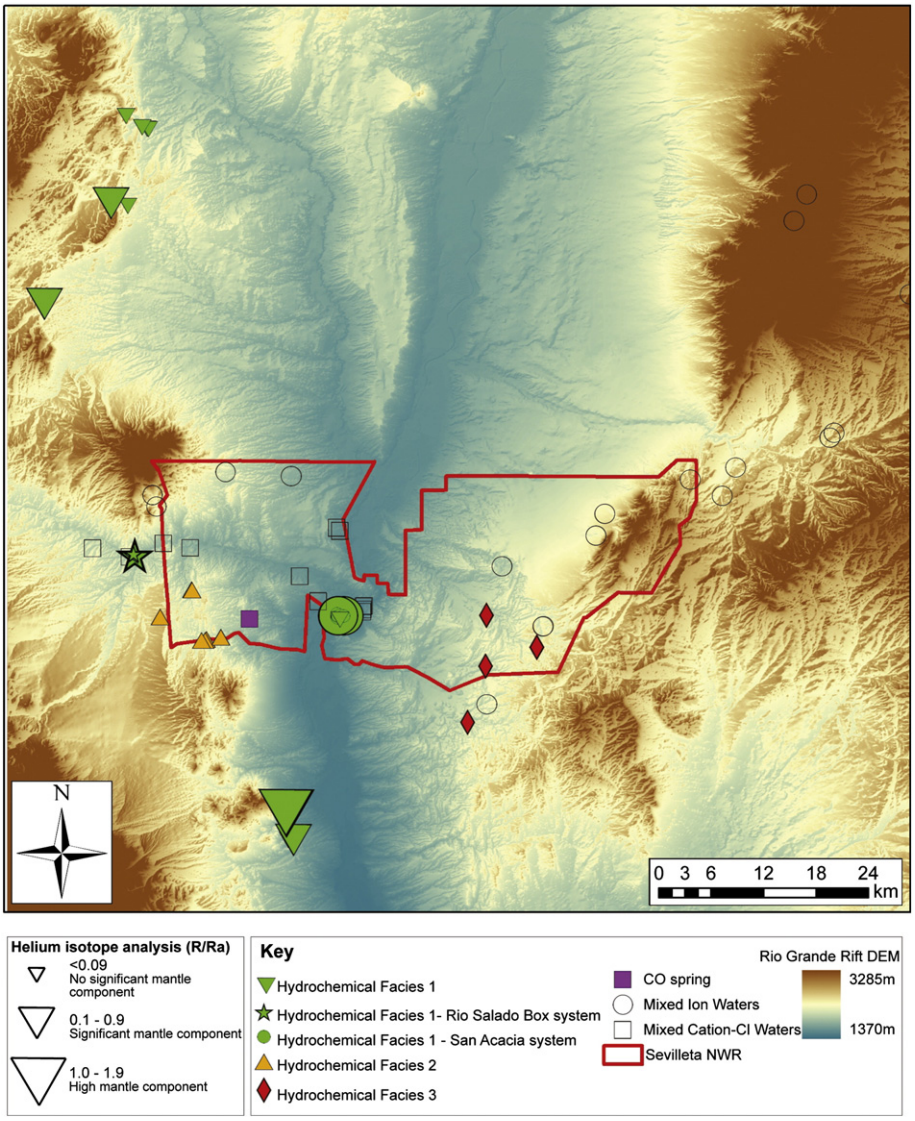

Fig. 8. Map of hydrochemical groups and relative location in the Rio Grande rift. Symbol sizes are scaled to R/Ra value. Symbols are the same as in Fig. 4.

The calculated percentages of the different sources of carbon (C_{carb}, $C_{organic}$, and $C_{endogenic}$) in each spring based on water chemistry and assumed endmember compositions are shown graphically in Fig. 9 (inset A). The mean values for each hydrochemical facies are identified in Fig. 9 as semi-filled symbols. The hydrochemical facies we defined are distinct, reinforcing our identification of mixing endmembers in the Rio Grande rift aquifers and showing regional water chemistry variations that reflect different percentages of endogenic inputs where a small flux of endogenic CO_2 carried by springs can significantly affect groundwater chemistry.

4.7. Evaporative concentration of salts in spring-fed brine pools

The nature and source of Na–Cl rich fluids in the western Rio Grande rift has been a topic of speculation for several decades (e.g. Goff et al., 1983). Rio Grande salinity levels greatly increase at San Acacia (Mills, 2003), and geochemical tracers in this study suggest that this region is a significant point source of endogenic fluids. Recently, elevated water temperatures (29 °C at ~159 m depth, corresponding to a geothermal gradient of 180 °C/km) were recorded from a San Acacia well (SAW), implying that flow rates are high enough to cause temperature anomalies (M. Person, Personal communication). The San Acacia spring/brine pool system must be examined in the context of the other waters from this study. We suggest that a small contribution from the highly saline San Acacia system can explain the observed salinity increase in the Rio Grande. This system contains multiple, close proximity spring vents and a line of evaporative pools that presently border the railroad grade and contain concentrated brines. The pool system is composed of upper, middle, and lower brine pools with conductivity increasing downstream.

The increasing conductivity correlates with the stable isotope composition of hydrogen and oxygen, confirming evaporative concentration of the brine pools. Stable isotopes of H and O indicate that meteoric water is a major component of the SNWR waters sampled, and that no magmatic waters are present (Fig. 10). Waters which plot to the right side of the local or global meteoric water line (LMWL or GMWL; Craig, 1961) do so due to evaporation, geothermal, or heavily circulated waters which undergo water–rock interaction with silicates, increasing $\delta^{18}O$ values while maintaining the δD values (Witcher et al., 2004). In geothermal fields, the geothermal and water–rock influenced waters will plot horizontally to the right of meteoric waters, while waters influenced by evaporation will plot with a slope of ~3 to 5 (e.g. Sharp, 2007). Several SNWR waters plot slightly to the right of both the GMWL and the Albuquerque LMWL (Plummer et al., 2004), which may indicate varying degrees of either evaporation and/or water–rock interaction with geothermal/deeply-derived fluids (Fig. 11).

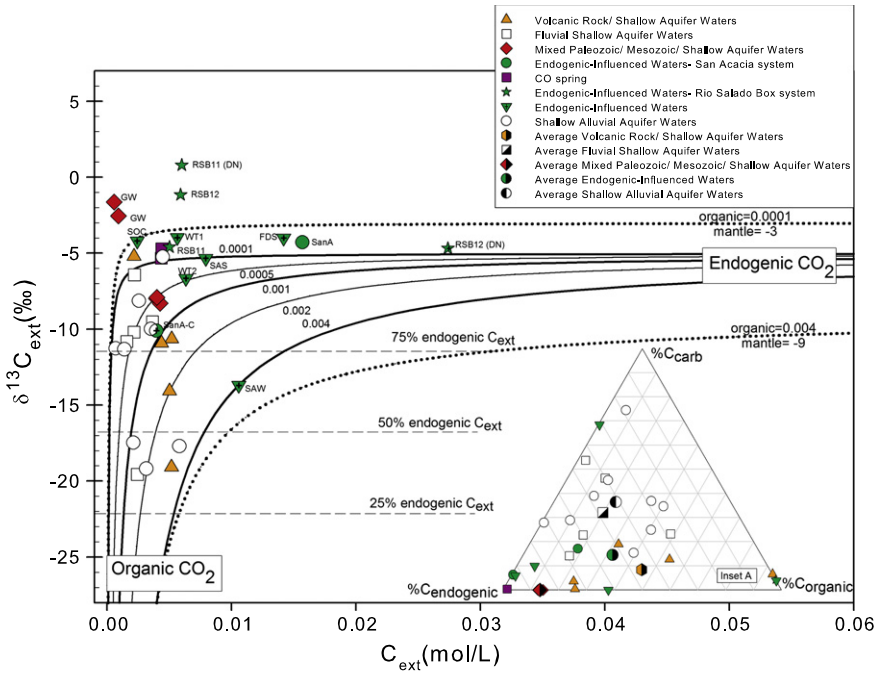

Fig. 9. Mixing model of $\delta^{13}C$ external versus $C_{external}$ for springs and surface waters from the SNWR. Model curves were chosen to encompass the majority of data points based on empirically derived endmembers: $\delta^{13}C_{organic} = -28‰$ and $\delta^{13}C_{endogenic} = -6‰$. Dashed lines represent a wider range for endogenic compositions ranging from $\delta^{13}C = -3‰$ to $-9‰$ (Sano and Marty, 1995). Samples with (DN) indicate collection and analysis from Newell, 2007. Inset A: The calculated percentages of the different sources of CO_2 (C_{carb}, $C_{organic}$, and $C_{endogenic}$) in each spring based on water chemistry and assumed endmember compositions are shown on a ternary diagram. The waters with high $C_{endogenic}$ percentages are the same as those previously identified that exhibit additional endogenic attributes based on multiple tracers. Symbols with a '+' sign represent $\delta^{13}C$ calculated from CO_2; all other samples represent $\delta^{13}C$ calculated from DIC.
Figure modified from Chiodini et al. (2004) and Crossey et al. (2009).

The San Acacia spring vents plot on the global meteoric water line, while the brine pool points fall well right of the meteoric water lines suggesting evaporation of the spring water (Fig. 11). An evaporation line can be fit from the spring to the lower brine pool to model the progressive evaporation of the brine pools. One of the San Acacia upper pool samples (SanA-S) is offset below the evaporation trend. This was sampled in the summer, and the resulting isotopic composition may demonstrate a mixture of evaporated spring water and meteoric water.

A mixing model of δD versus [Cl] was developed to demonstrate the proportion of saline fluid from the San Acacia system required to produce the chemistry observed immediately downstream in the Rio Grande (Fig. 11). Models mixed both the San Acacia spring and the San Acacia upper brine pool (SanA) with the Rio Grande (RG) to determine the percent mixture required to produce the salinity measured downstream of both at the San Acacia Diversion Dam (DD). The model indicates that a mix of 5% of the San Acacia upper brine pool and/or a mix of ~10% of the San Acacia spring water with the Rio Grande will yield the downstream [Cl], suggesting a slow underground seep of briny water from the San Acacia system to the river. This model indicates that a small contribution from the highly saline San Acacia system can explain the observed salinity increase in the Rio Grande (Mills, 2003).

Although calculated halite saturation indices indicate that the San Acacia system is not supersaturated with respect to halite at the surface (see Supplementary Material Table 4), the high Cl/Br ratios of the system may be explained by the presence of halite at depth. Additionally, salt-encrusted soil and plants are pervasive in the area surrounding the spring system and buried salt crusts from past floodplains may be present. Most other waters in the Sevilleta system are characterized by low Cl/Br ratios and [Cl], suggesting that they are influenced by separate rift flowpaths that do not carry the deeply-derived salt signature.

4.8. Importance of new hydrologic flow and hydrochemical facies models

A geologic framework combined with these geochemical datasets (Fig. 2A) is used to interpret the dominant flow paths of the Rio Grande rift groundwaters near the SNWR transect. Potentiometric lines for epigenic waters as modeled by Plummer et al. (2004) (Fig. 3B) show recharge and shallow infiltration from snow melt and rainfall along both rift flanks. Similar flow paths can explain the geochemistry of hydrochemical facies 2 and 3, as HCO_3-dominated waters correspond with volcanic substrate and SO_4-dominated waters correspond with evaporite substrate. Flow paths, denoted as arrows on Fig. 2A, suggest that many of the shallow wells in these regions will be dominated by mixtures of epigenic waters in shallow flowpaths with compositionally distinct endogenic fluids. As discussed earlier, deep circulation and southward flow parallel to the Rio Grande (Fig. 3A) is also a possible flow path for old slow-moving basin brines, although we propose that emergence of such fluids along basin constrictions would be strongly influenced by the faults shown in Fig. 2. Furthermore, deep basin brines are more likely to be tapped by fault-parallel flow than the deep circulation systems depicted in Fig. 3A.

New aspects of our hydrologic model concentrate on high permeability pathways and fluid mixing along rift faults. Springs along basin-bounding and intra-rift faults indicate zones of discharge and preliminary modeling suggests that these faults are several orders of magnitude more permeable than the crystalline bedrock (Woolsey et al., 2012). Flow along these faults may locally dominate over either the Plummer et al. (2004)- or Mills (2003)-type circulation systems (Fig. 3A, B). Although moderately cemented faults in the region (e.g. the Sand Hill fault) may exhibit lower permeability locally (>8% calcite cement may significantly affect permeability; Davis et al., 2006), these cemented areas are locally discontinuous features (Davis et al., 2006) and their cross-fault permeability can evolve through time (Rawling et al., 2001). We suggest that anisotropically permeable faults will

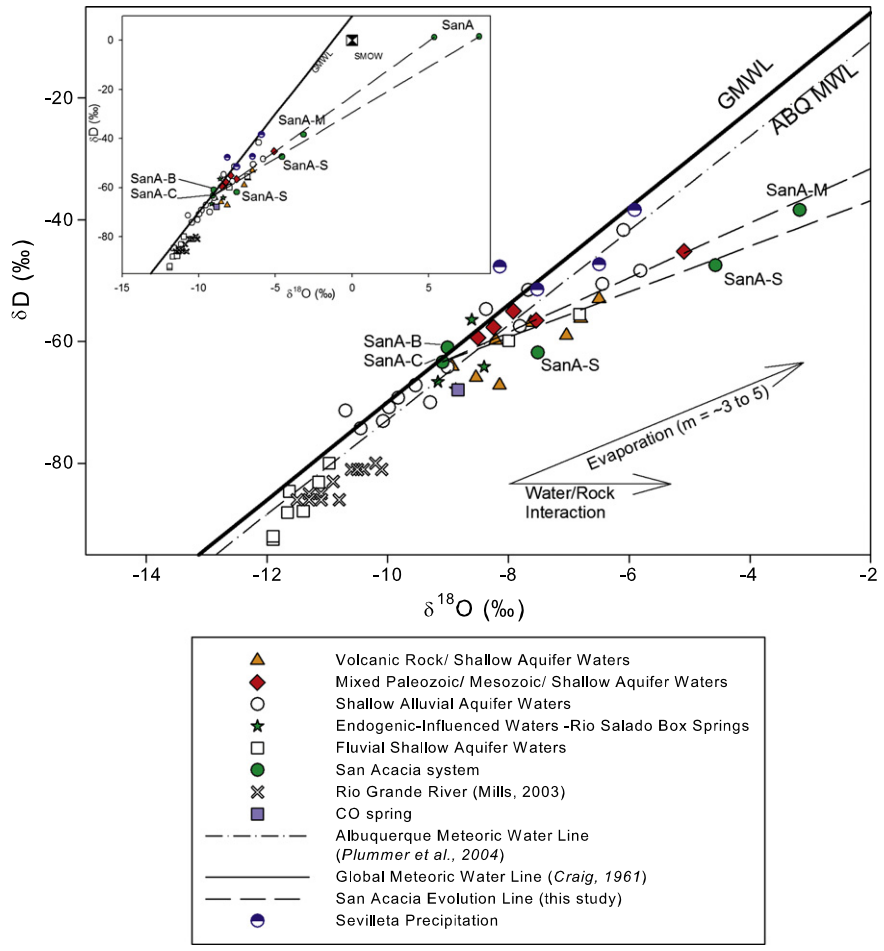

Fig. 10. Stable isotopes of ^{18}O and D for all SNWR waters and the extent of the Rio Grande in the SNWR (from Mills, 2003). SanA-B, SanA-C = San Acacia spring vents, SanA-S = northernmost upper pool, SanA-M = middle pool, SanA = southernmost lower pool. Waters which plot to the left of the GMWL may have seen post-collection geochemical influences due to condensation.

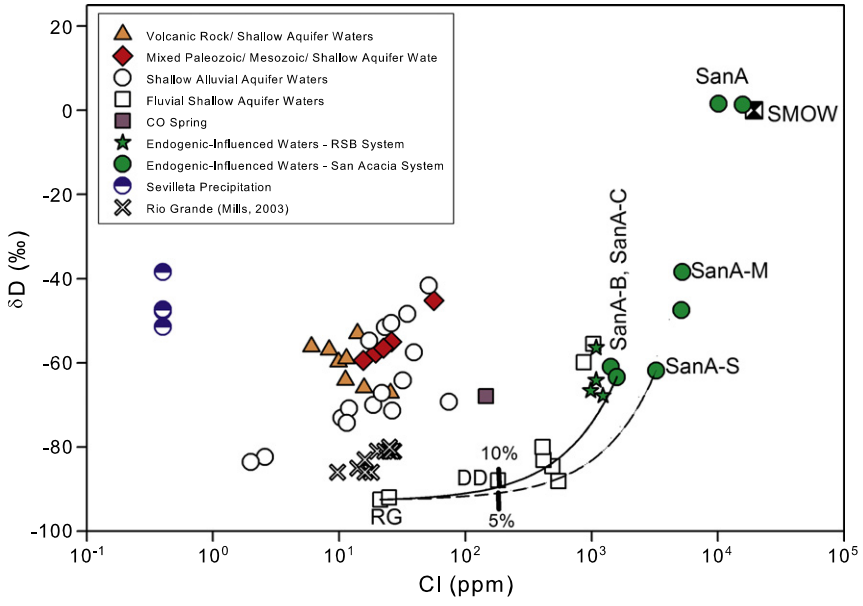

Fig. 11. Mixing model of δD versus [Cl]. The model indicates that a mix (dashed line) of 5% San Acacia upper brine pool (SanA-S) and/or a mix (solid line) of 10% San Acacia spring water with the Rio Grande (RG) above the San Acacia confluence will yield the geochemistry observed downstream at the San Acacia Diversion Dam (DD), indicating that a small contribution from the highly saline San Acacia system may contribute to Rio Grande salinization. SMOW is Standard Mean Ocean Water (Craig, 1961).

impede lateral groundwater flow between sub-basins and strongly enhance vertical fluid flow and mixing up faults (Bense and Person, 2006). As shown in Fig. 2, geochemical evidence suggests a flow of endogenic fluid up faults to form endogenic fluid point sources at certain springs. Modeling results illustrate the importance and necessity of a deeply penetrating, relatively permeable conduit/fault zone, such as in Fig. 2, to explain advective transport of primordial ^{3}He through the ductile boundary to shallow crustal levels (Woolsey et al., 2012). This is analogous to geothermal fluid circulation seen at the Coso and Beowawe hydrothermal systems (Banerjee et al., 2011).

Fig. 2B portrays the larger spatial scale of endogenic fluid circulation, and the various likely components of the conduit system. Mantle-derived fluids ascend upwelling limbs of hydrothermal systems related to the Socorro magma body. Local seismic activity related to the Socorro Seismic Anomaly (Reiter, 2005) may enhance fracture permeability in the upper 11 km of crust, even below the brittle–ductile transition at 5–8 km when deeper shear zones and fractures form during large rupture events. We argue for a strong association between high [CO_2] springs, faults, an active magma body associated microseismicity, and mantle degassing based on the observations that the endogenically-influenced Hydrochemical facies 1 springs are along faults, contain mantle helium and are high in [CO_2]. This is similar to other studies that assumed a magmatic origin for some or most of the high [CO_2] in regional groundwaters, springs, and gas fields (Ballentine et al., 2002; Gilfillan et al., 2008; Crossey et al., 2009; Gilfillan et al., 2009; Karlstrom et al., 2013). We speculate that CO_2 degassing above the magma interacts with microseismicity in a feedback system where fluids enhance fault rupture and fault rupture promotes ascent of fluids. Exsolution of CO_2 as a separate gas phase takes place in the upper 1 km of the crust, and phase separation of supercritical CO_2 from hydrous fluids can occur at deeper levels, depending on temperature and pressure conditions. This CO_2 degassing and re-dissolution greatly influences the $\delta^{13}C$ and $CO_2/^3He$ values of surface springs. The values reported here generally reflect a crustal fractionation history (Gilfillan et al., 2008), consistent with our interpretations.

Deconvolving this CO_2 fractionation history is not possible given existing data, but $CO_2/^3He$ ratios offer some clues. $CO_2/^3He$ values measured on our samples (Table 1) vary over 6 orders of magnitude, from 10^7 to 10^{13}. Our average value of 3.93×10^{12} is 2 to 3 orders of magnitude higher than $CO_2/^3He$ of MORB (1×10^9 to 1×10^{10}) (Marty and Jambon, 1987), and our values are similar to other continental regions that also show large variability (O'Nions and Oxburgh, 1988). Some of the springs such as the Rio Salado Box springs and Coyote fault wells have values of $6–9 \times 10^9$ that are within the range of MORB values, such that a significant component of magmatic CO_2 is inferred. However, most samples show CO_2 enrichment, likely from multiple sources (Baines and Worden, 2004) and crustal fractionation processes, such as CO_2/water phase partitioning with groundwater (Gilfillan et al., 2008). In contrast, the New Mexico Tech geothermal well groundwaters show CO_2 depletion relative to MORB values that can be explained as a residual from CO_2 loss or fractionation that took place after magmatic degassing (Sherwood Lollar et al., 1997; Gilfillan et al., 2008). It is the upward movement of initially magmatic-derived carbonic fluids that we envision to be driving the entrainment of brines, and upper crustal mixing of different hydrochemical facies to produce the variable hydrochemistry observed in the Rio Grande rift. Our model views the shallow aquifer as variably mixed with these endogenic influences and thus degassing may cause carbonate cementation in the aquifer and hence affect local aquifer and fault permeability.

All of the tracers discussed above consistently identify the same springs as point sources of fluids containing anomalous inputs of water quality-degrading salts and metals. For water supply management, our new hydrologic model highlights the importance of understanding water volumes and chemistries of these chemically potent point sources. Our mixing trends suggest that even small volume discharge from known vents can affect water quality, and there is potential for subsurface leakage of endogenic waters into large regions of the Santa Fe Group aquifer. This hydrologic model emphasizes the importance of better understanding rift faults for both flow models and water quality assessment.

4.9. Future modeling directions

The recognition of the presence and importance of endogenic fluid inputs into the Albuquerque basin shallow aquifers is a major goal of this paper. In this work, we do not extend the analysis to attempt to define mixing proportions and flow paths, but such future work is possible. Currently, researchers are developing flow models that estimate mixing percentages, and we look forward to better defined mixing proportions and flow paths once hydrologic models recognize the presence and importance of endogenic fluids. In the future we envision geochemical aquifer characterization that emphasizes the importance of pinpointing endogenic inputs. Poor water quality endogenic fluids can then be mitigated via mixing with better quality water. Future hydrologic flow models need to prospect for downwelling cells of fault parallel circulation systems and to avoid the lower water quality of upward flowing cells.

At the southern terminus of the Albuquerque Basin, an important modeling constraint is that flow rates along fault zones need to be high enough to produce the observed $^3He/^4He$ anomalies and yet slow enough to not generate significant thermal anomalies at springs in the San Acacia area. Preliminary data suggest fault permeabilities that are several to ten times matrix permeability would be reasonable to satisfy this criterion (Woolsey et al., 2012). Application of variable-density groundwater, heat, stable isotope, noble-gas, and brine transport models (e.g. Banerjee et al., 2011) could be used to quantify the contribution of deep endogenic fluids to shallow geochemical anomalies along the southern Albuquerque Basin reported in this study. Hydrologic modeling could also be used to evaluate whether diffuse groundwater discharge across shallow Paleozoic and Tertiary confining units (such as those associated with hydrochemical facies 3 waters), driven by along-rift-axis hydraulic gradients, are sufficiently high to tilt the brine–water contact at the southern margin of the basin (Park et al., 2009) and produce the salinity increases observed within the Rio Grande versus whether fault-controlled fluid flow is required. Idealized models might also help constrain the age of emplacement of the Socorro magma body by determining the minimum time required for endogenic fluids to arrive at the surface without transporting significant amounts of heat.

5. Conclusions: a tectonic component to saline ground and surface waters

This study applies multiple geochemical tracers to both surface and groundwaters in a transect across the Rio Grande rift. The range of water chemistry we observe is representative of water compositions for the entire Albuquerque hydrologic basin such that our models may be generalized to the entire basin and perhaps to other arid regions. We present the following conclusions:

(1) Marked variations in water chemistry can be explained by mixing of small volumes of geochemically potent endogenic (deeply-derived) fluids with the volumetrically dominant epigenic waters (dominated by meteoric recharge). Endogenic fluids have variable compositions and three geographically distinct hydrochemical facies compositions were identified with varying endogenic fluid contributions. Hydrochemical facies 1 waters are Na–Cl waters that correlate with elevated temperatures, conductivity, TDS, [Cl], $^{87}Sr/^{86}Sr$ ratios, trace metals, and mantle helium signatures, and include CO_2-exsolving springs on large rift-bounding faults, wells along the Rio Salado, and intra-rift fault springs near San Acacia. The mixing trend is interpreted to reflect mixing of endogenically-influenced

fault-related fluids (possibly including hydrothermal and magmatically influenced fluids) with meteoric inputs. Hydrochemical facies 2 waters are SNWR southwest-specific mixed cation–HCO_3 waters that correlate with low temperature, conductivity, TDS, [Cl], Cl/Br, $^{87}Sr/^{86}Sr$ ratios and depleted $\delta^{13}C$ signatures are interpreted as meteoric water interacting with local volcanic units (e.g. rhyolite of the La Jencia tuff; Chamberlain et al., 2004), and/or volcaniclastic rift fill sediments to form volcanic rock/fractured shallow aquifer waters. Hydrochemical facies 3 waters are SNWR southeast-specific Ca–SO_4 waters that correlate with low temperature, [Cl], Cl/Br, and $^{87}Sr/^{86}Sr$ ratios, and elevated conductivity, TDS, and [SO_4]. These are interpreted to be mixed Paleozoic/Mesozoic/shallow aquifer waters formed from leaching of the Permian Abo and gypsum-rich Yeso Formations along a series of small NE–SW trending faults and subsequently mixed with meteoric water. They may reflect endogenic waters derived in part from basin brines associated with Paleozoic evaporites.

(2) Several point source endogenic springs from Hydrochemical facies 1 are identified based on multiple tracers; these show a correspondence of high $^3He/^4He$, high $^{87}Sr/^{86}Sr$, high [Cl], high trace metal concentrations, high P_{CO_2}, warm temperatures, and higher $\delta^{13}C$ values. The ^3He, a significant fraction of the CO_2, and perhaps some of the Cl and trace metals are interpreted to have come from deep magmatic sources. Elevated $^{87}Sr/^{86}Sr$ ratios, additional trace metals, and additional Cl are interpreted to reflect crustal water–rock interaction, including entrainment of basin brine in ascending endogenic fluids.

(3) Waters of Hydrochemical facies 3 show the influence of basin brines (potentially from the Permian Yeso Formation and/or evolved seawater). These are similar to waters in other areas where Yeso evaporites are in the shallow subsurface such as along the Comanche Fault and in the Sacramento Mountains in south central New Mexico (Rawling et al., 2008).

(4) The San Acacia spring and evaporative pools are a point source for increased salinization along the Rio Grande. Endogenic spring waters upwell along an intra-rift fault and our geologic model suggests that salinization of the river at this and other basin constrictions is due to a two stage process where faults convey salt-bearing endogenic waters to spring vents, then evaporative pools further concentrate salts into brines that leak into the river and groundwater system. Brine pool evaporation is supported by Cl/Br ratios and $\delta^{18}O/\delta D$ isotope modeling to reflect modification of endogenic-influenced spring water.

(5) Faults serve as zones of endogenic water upwelling and as high permeability domains in the aquifer. Several springs deserve special mention; from north to south, Coyote Spring (0.870 R_A), Four Daughters Spring (0.587 R_A), Rio Salado Box springs (0.370 R_A), San Acacia spring (0.256 R_A), and the New Mexico Tech geothermal well (1.907 R_A) all have $^3He/^4He$ ratios above 0.1 R_A providing evidence for mantle fluids entrained in the groundwater system. These springs are also all above ambient temperature, CO_2-rich, and are interpreted to be influenced by geothermal fluids (Newton, 2004; Hogan et al., 2007).

(6) Endogenic waters carry trace metals and salts that significantly degrade water quality. This has an underappreciated importance for the Santa Fe Group aquifer system and Rio Grande rift hydrology. Combined geochemical and hydrologic studies provide a constructive direction for the mitigation of point sources of water degradation at surface springs and also provide new insight for isolating wells that might tap into endogenic waters that could then be isolated and mitigated. New research steps involve application of multiple tracers to estimate mixing volumes and times of transport of different endogenic and epigenic endmembers.

Supplementary data to this article can be found online at http://dx.doi.org/10.1016/j.chemgeo.2013.05.029.

Acknowledgments

This research was partially supported by the National Science Foundation through the Hydrologic Sciences Program (NSF EAR 0538304 and 0838575 to Crossey and Karlstrom) and by a National Science Foundation grant to the University of New Mexico for Long-term Ecological Research (NSF-DEB-0620482 to Collins) at the Sevilleta National Wildlife Refuge; and student grants from the National Science Foundation Long Term Ecological Research Program at the Sevilleta National Wildlife Refuge (DEB-0620482) (Williams), the New Mexico Water Resources Research Institute W09010 (Williams/Crossey), the New Mexico Geological Society (Williams), the University of New Mexico Office of Graduate Studies Research, Projects, and Travel grant (Williams), the University of New Mexico Graduate and Professional Student Association Student Research Allocations Committee award (Williams), and the University of New Mexico Department of Earth & Planetary Sciences. Thanks go to the personnel from the U.S. Fish & Wildlife Services at the Sevilleta NWR and Sevilleta LTER researchers, staff, 2008/2009 REU students, 2007–2009 UNM graduate students, J. Copeland for assistance with Coyote Fault well sampling, and Souder, Miller and Associates for San Acacia well samples and well log data. Thanks to A. Ali and K. Guggliota for assistance in analytical chemistry, to V. Atudiori for stable isotope analysis assistance, and to V. Polyak for radiogenic isotope analysis assistance. Thanks also go to Y. Asmerom and S. Elardo for helpful suggestions, and to two anonymous reviewers whose comments greatly improved this manuscript.

References

Anderson, A.T., 1974. Chlorine sulfur and water in magmas and oceans. Geological Society of America Bulletin 85, 1485–1492.

Andrews, J.N., 1985. The isotopic composition of radiogenic helium and its use to study groundwater movements in confined aquifers. Chemical Geology 49, 339–351. http://dx.doi.org/10.1016/0009-2541(85)90166-4.

Anning, D.W., Bauch, N.J., Garner, S.J., Flynn, M.E., Hamlin, S.N., Moore, S.J., Schaefer, D.H., Anderholm, S.K., Spangler, L.E., 2007. Dissolved solids in basin-fill aquifers and streams in the southwestern United States. US Geological Survey Scientific Investigations Report 2006–2515.

Bachman, G.O., Mehnert, H.H., 1978. New K–Ar dates and the late Pliocene to Holocene geomorphic history of the central Rio Grande region, New Mexico. Geological Society of America Bulletin 89, 283–292.

Baines, S.J., Worden, R.H., 2004. The long term fate of CO_2 in the subsurface: natural analogues for CO_2 storage. In: Baines, S.J., Worden, R.H. (Eds.), Geological Storage of Carbon Dioxide: Geological Society, 233, pp. 59–85.

Balch, R.S., Hartse, H.E., Sanford, A.R., Lin, K., 1997. A new map of the geographic extent of the Socorro magma body. Seismological Society of America Bulletin 87, 174–182.

Ballentine, C.J., Burnard, P.G., 2002. Production, release and transport of noble gases in the continental crust. In: Porcelli, D., Ballentine, C.J., Weiler, R. (Eds.), Reviews in Mineralogy and Geochemistry — Noble Gases in Geochemistry and Cosmochemistry, 47. Mineralogical Society of America, Washington, D.C., pp. 481–538.

Ballentine, C.J., Burgess, R., Marty, B., 2002. Tracing fluid origin, transport and interaction in the crust. In: Porcelli, D., Ballentine, C.J., Wieler, R. (Eds.), Reviews in Mineralogy and Geochemistry — Noble Gases in Geochemistry and Cosmochemistry, 47. Mineralogical Society of America, Washington, D.C., pp. 539–614.

Banerjee, A., Person, M., Hofstra, A., Sweetkind, D., Cohen, D., Unruh, J., Zyvoloski, G., Gable, C.W., Crossey, L., Karlestrom, K., 2011. Fault controlled helium transport and fluid–rock isotope exchange in the Great Basin, USA. Geology 39, 195–198.

Barrett, J.K., Pearl, R.H., 1978. An appraisal of Colorado's geothermal resources. Colorado Geological Survey Bulletin 39, 224 p.

Bense, V.F., Person, M.A., 2006. Faults as conduit–barrier systems to fluid flow in siliciclastic sedimentary aquifers. Water Resources Research 42 (W05421).

Bexfield, L.M., Plummer, L.N., 2003. Occurrence of arsenic in ground water of the middle Rio Grande Basin, central New Mexico. In: Welch, A.H., Stollenwerk, K.G. (Eds.), Arsenic in Ground Water: Geochemistry and Occurrence. Kluwer Academic Publishers, pp. 295–327.

Bottomley, D.J., Gregoire, D.C., Raven, K.G., 1994. Saline ground waters and brines in the Canadian Shield: geochemical and isotopic evidence for a residual evaporite brine component. Geochimica et Cosmochimica Acta 58, 1483–1498.

Brand, U., 2004. Carbon, oxygen and strontium isotopes in Paleozoic carbonate components: an evaluation of original seawater-chemistry proxies. Chemical Geology 204, 23–44.

Burke, W.H., Denison, R.E., Hetherington, E.A., Koepnick, R.B., Nelson, H.F., Otto, J.B., 1982. Variation of seawater $^{87}Sr/^{86}Sr$ throughout Phanerozoic time. Geology 10, 516–519.

Caine, J.S., Minor, S.A., 2009. Structural and geochemical characteristics of faulted sediments and inferences on the role of water in deformation, Rio Grande Rift, New Mexico. Geological Society of America Bulletin 121, 1325–1340.

Chamberlain, R.M., McIntosh, W.C., Eggleston, T.L., 2004. $^{40}Ar/^{39}Ar$ geochronology and eruptive history of the eastern sector of the Oligocene Socorro caldera, central Rio Grande rift, New Mexico. New Mexico Bureau Geology Mines Resources Bulletin 160, 251–279.

Chapin, C.E., Cather, S.M., 1994. Tectonic setting of axial basins of the Northern and Central Rio Grande Rift. In: Keller, G.R., Cather, S.M. (Eds.), Basins of the Rio Grande Rift: Structure, Stratigraphy, and Tectonic Setting: Geological Society of America Special Paper, 291, pp. 5–25.

Chiodini, G., Frondini, F., Cardellini, C., Parello, F., Peruzzi, L., 2000. Rate of diffuse carbon dioxide Earth degassing estimated from carbon balance of regional aquifers: the case of central Apennine, Italy. Journal of Geophysical Research 105, 8423–8434.

Chiodini, G., Cardellini, C., Amato, A., Boshi, E., Caliro, S., Frondini, F., Ventura, G., 2004. Carbon dioxide Earth degassing and seismogenesis in central and southern Italy. Geophysical Research Letters 31 (L07615).

Clarke, W.B., Beg, M.A., Craig, H., 1969. Excess ^{3}He in the sea: evidence for terrestrial primordial helium. Earth and Planetary Science Letters 6, 213–220. http://dx.doi.org/10.1016/0012-821X(69)90093-4.

Craig, H., 1961. Isotopic variations in meteoric waters. Science 133, 1702–1703.

Craig, H., Lupton, J.E., Welhan, J.A., Poreda, R.J., 1978. Helium isotopic ratios in Yellowstone and Lassen Park volcanic gases. Geophysical Research Letters 5, 897–900. http://dx.doi.org/10.1029/GL005i011p00897.

Crossey, L.J., Fischer, T.P., Patchett, P.J., Karlstrom, K.E., Hilton, D.R., Newell, D.R., Huntoon, P., 2006. Dissected hydrologic system at the Grand Canyon: interaction between deeply derived fluids and plateau aquifer waters in modern springs and travertine. Geology 34, 25–28.

Crossey, L.J., Karlstrom, K.E., Springer, A., Newell, D., Hilton, D.R., Fischer, T., 2009. Degassing of mantle-derived CO_2 and He from springs in the southern Colorado Plateau region—neotectonic connections and implications for groundwater systems. Geological Society of America Bulletin 121, 1034–1053.

Davis, S.N., Whittemore, D.O., Fabryka-Martin, J., 1998. Uses of chloride/bromide ratios in studies of potable water. Ground Water 36, 338–350.

Davis, J.M., Roy, N.D., Mozley, P.S., Hall, J.S., 2006. The effect of carbonate cementation on permeability heterogeneity in fluvial aquifers: an outcrop analog study. Sedimentary Geology 184, 267–280.

De Moor, M., Zinsser, A., Karlstrom, K.E., Chamberlin, R., Connell, S., Read, A., 2005. Preliminary geologic map of the La Joya 7.5-minute quadrangle, Socorro County, New Mexico. New Mexico Bureau of Mines and Mineral Resources (Open-file Geologic Map OF-GM 102, scale 1:24,000).

Deines, P., Langmuir, D., Harmon, R.S., 1974. Stable carbon isotope ratios and the existence of a gas phase in the evolution of carbonate ground waters. Geochimica et Cosmochimica Acta 38, 1147–1164.

Doremus, D., Lewis, G., 2008. Rio Grande salinity management — a real possibility? SW Hydrology 7, 24–25.

Drever, J.L., 1997. The Geochemistry of Natural Waters: Surface and Groundwater EnvironmentsThird ed. Prentice-Hall, New Jersey.

Dunai, T.J., Porcelli, D., 2002. Storage and transport of noble gas in the subcontinental lithosphere. In: Porcelli, D., Ballentine, C.J., Wieler, R. (Eds.), Reviews in Mineralogy and Geochemistry — Noble Gases in Geochemistry and Cosmochemistry, 47. Mineralogical Society of America, Washington, D.C., pp. 371–409.

Dunbar, N.W., 2005. Quaternary volcanism in New Mexico, in New Mexico's Ice Ages. In: Lucas, S.G., Morgan, G.S., Zeigler, K.E. (Eds.), New Mexico Museum of Natural History Scientific Bulletin: , 28.

Earman, S., Phillips, F.M., McPherson, B., 2005. The role of "excess" CO_2 in the formation of trona deposits. Applied Geochemistry 20, 2217–2232. http://dx.doi.org/10.1016/j.apgeochem.2005.08.007.

Faure, G., 1998. Principles and Applications of GeochemistrySecond ed. Prentice-Hall, New Jersey.

Fialko, Y., Simons, M., 2001. Evidence for on-going inflation of the Socorro Magma Body, New Mexico, from interferometric synthetic aperture radar imaging. Geophysical Research Letters 28, 3549–3552. http://dx.doi.org/10.1029/2001GL013318.

Fontes, J.C., Garnier, J.M., 1979. Determination of the initial ^{14}C activity of the total dissolved carbon: a review of the existing models and a new approach. Water Resources Research 5, 399–413.

Fontes, J.Ch., Matray, J.M., 1993. Geochemistry and origin of formations brines from the Paris Basin, France: 2. Saline solutions associated with oil fields. Chemical Geology 109, 177–200.

Ghassemi, F., Jakeman, A.J., Nix, H.A., 1995. Salinisation of Land and Water Resources: Human Causes, Extent, Management and Case Studies. CAB International, Wallingford, UK.

Gilfillan, S.M., Ballentine, C., Holland, G., Blagburn, D., Lollar, B.S., Stevens, S., Schoell, M., Cassidy, M., 2008. The noble gas geochemistry of natural CO_2 gas reservoirs from the Colorado Plateau and Rocky Mountain provinces, USA. Geochimica et Cosmochimica Acta 72, 1174–1198.

Gilfillan, S.M., Sherwood-Lollar, S., Holland, G., Blagburn, D., Stevens, S., Schoell, M., Cassidy, M., Ding, Z., Lacrampe-Couloume, G., Ballentine, C.J., 2009. Solubility trapping in formation water as dominant CO_2 sink in natural gas fields. Letters to Nature 458, 614–618.

Goff, F., McCormick, T., Gardner, J.N., Trujillo, P.E., Counce, D., Vidale, R., Charles, R., 1983. Water Geochemistry of the Lucero Uplift, New Mexico.Los Alamos National Laboratory 26.

Graham, D.W., 2002. Noble gas isotope geochemistry of mid-ocean ridge and ocean island basalts: characterization of mantle source reservoirs. In: Porcelli, D., Ballentine, C.J., Weiler, R. (Eds.), Reviews in Mineralogy and Geochemistry — Noble Gases in Geochemistry and Cosmochemistry, 47. Mineralogical Society of America, Washington, D.C., pp. 451–538.

Hibbs, B., Merino, M., 2007. Discovering a geologic salinity source in the Rio Grande aquifer. SW Hydrology 20–21, 33.

Hilton, D.R., 1996. The helium and carbon isotope systematics of a continental geothermal system: results from monitoring studies at Long Valley caldera (California, U.S.A.). Chemical Geology 127, 269–295.

Hogan, J.F., Phillips, F.M., Mills, S.K., Hendrickx, J.M.H., Ruiz, J., Chesley, J.T., Asmerom, Y., 2007. Geologic origins of salinization in a semi-arid river: the role of sedimentary basin brines. Geology 35, 1063–1066.

Hurst, R.W., 2003. Isotopic tracers in groundwater hydrology. SW Hydrology 2.

Karlstrom, K., Crossey, L., Hilton, D., Barry, P., 2013. Mantle ^{3}He and CO_2 degassing in carbonic and thermal springs of Colorado and implications for neotectonics of the Rocky Mountains. Geology 41, 495–498.

Keller, G.R., Baldridge, W.S., 1999. The Rio Grande rift: a geological and geophysical overview. Rocky Mountain Geology 34, 121–130.

Kendrick, M.A., Woodhead, J.D., Kamenetsky, V.S., 2012. Tracking halogens through the subduction cycle. Geology 40, 1075–1078.

Kennedy, B.M., Lynch, M.A., Reynolds, J.H., Smith, S.P., 1985. Intensive sampling of noble gases in fluids at Yellowstone: I. Early overview of the data; regional patterns. Geochimica et Cosmochimica Acta 49, 1251–1261. http://dx.doi.org/10.1016/0016-7037(85)90014-6.

Kennedy, B.M., Reynolds, J.H., Smith, S.P., 1987. Helium isotopes: Lower Geyser Basin, Yellowstone National Park. Journal of Geophysical Research 92, 12477–12489. http://dx.doi.org/10.1029/JB092iB12p12477.

Kennedy, B.M., Kharaka, Y.K., Evans, W.C., Ellwood, A., DePaolo, D.J., Thordsen, J., Ambats, G., Mariner, R.H., 1997. Mantle fluids in the San Andreas fault system, California. Science 278, 1278–1281. http://dx.doi.org/10.1126/science.278.5341.1278.

Kennedy, B.M., Torgersen, T., van Soest, M.C., 2002. Multiple atmospheric noble gas components in hydrocarbon reservoirs: a study of the northwest shelf, Delaware Basin, SE New Mexico. Geochimica et Cosmochimica Acta 66, 2807–2822.

Land, L.S., Prezbindowski, D.R., 1981. The origin and evolution of saline formation water, Lower Cretaceous carbonates, south-central Texas, USA. Journal of Hydrology 54, 51–74.

Larsen, S.R., Reilinger, R., Brown, L., 1986. Evidence of ongoing crustal deformation related to magmatic activity near Socorro, New Mexico. Journal of Geophysical Research 91, 6283–6293.

Lewis, C.J., Baldridge, W.S., 1994. Crustal extension in the Rio Grande rift, New Mexico: half-grabens, accommodation zones, and shoulder uplifts in the Ladron Peak-Sierra Lucero area. Geological Society of America Special Paper 291, 135–155.

Lippencott, J.B., 1939. Southwest border water problems. Journal of American Water Works Association 31, 1–28.

Liu, Z., Zhang, M., Li, Q., You, S., 2003. Hydrochemical and isotopic characteristics of spring water and travertine in the Baishuitai area (SW China) and their meaning for paleoenvironmental reconstruction. Environmental Geology 44, 698–704.

Machette, M.N., Personius, S.F., Kelson, K.I., Dart, R.L., Haller, K.M., 2000. Map and data for Quaternary faults and folds in New Mexico. U.S. Geological Survey (Open File Report 98-0521).

Mailloux, B.J., Person, M., Kelley, S., Dunbar, N., Cather, S., Strayer, Q., Hudleston, P., 1999. Tectonic controls on the hydrogeology of the Rio Grande Rift, New Mexico. Water Resources Research 35, 2641–2659.

Marty, B., Jambon, A., 1987. $C/^{3}He$ in volatile fluxes from the solid Earth: implications for carbon geodynamics. Earth and Planetary Science Letters 83, 16–26.

May, S.J., Russell, L.R., 1994. Thickness of the synrift Santa Fe Group in the Albuquerque basin and its relation to structural style. Geological Society of America Special Paper 291, 113–123.

Mills, S.K., 2003. Quantifying Salinization of the Rio Grande Using Environmental Tracers. (M.S. Thesis) New Mexico Institute of Mining and Technology (397 pp.).

Moore, S.J., Bassett, R.L., Liu, B., Wolf, C.P., Doremus, D., 2008. Geochemical tracers to evaluate hydrogeologic controls on river salinization. Ground Water 46, 489–501.

Mozley, P.S., Goodwin, L.B., 1995. Patterns of cementation along a Cenozoic normal fault: a record of paleoflow orientations. Geology 23, 539–542.

Mukhopadhyay, B., Brookins, D.G., 1976. Strontium isotope composition of the Madera Formation (Pennsylvanian) near Albuquerque, New Mexico. Geochimica et Cosmochimica Acta 40, 611–616.

Muramatsu, Y., Wedepohl, K.H., 1979. Chlorine in tertiary basalts from the Hessian Depression in N–W Germany. Contributions to Mineralogy and Petrology 70, 357–366.

Musgrove, M., Banner, J.L., 1993. Regional ground-water mixing and the origin of saline fluids: midcontinent, United States. Science 259, 1877–1882.

Newell, D.L., 2007. Hydrogeochemistry of CO_2-rich mineral springs: implications for tectonics and microbiology. (Ph.D. Dissertation) University of New Mexico (156 pp.).

Newell, D.L., Crossey, L.J., Karlstrom, K.E., Fischer, T.P., 2005. Continental-scale links between the mantle and groundwater systems of the western United States: evidence from travertine springs and regional He isotope data. GSA Today 15, 4–10.

Newton, B.T., 2004. Geologic Controls on Shallow Groundwater Quality in the Socorro Basin, New Mexico. (M.S. Thesis) New Mexico Institute of Mining and Technology (163 pp.).

O'Nions, R.K., Oxburgh, E.R., 1988. Helium, volatile fluxes and the development of continental crust. Earth and Planetary Science Letters 90, 331–347.

Osburn, G.R., 1984. Geologic map of Socorro County. New Mexico Bureau of Mines and Mineral Resources (Open File Report 238).

Park, Y.-J., Sudicky, E.A., Sykes, J.F., 2009. Effects of shield brine on the safe disposal of waste in deep geologic environments. Advances in Water Resources 32, 1352–1358.

Parkhurst, D.L., Appelo, C.A.J., 1999. User's guide to PHREEQC—a computer program for speciation, reaction-path, 1D-transport, and inverse geochemical calculations. U.S. Geological Survey Water Resources Investigations Report 1999–4259.

Patchett, P.J., Spencer, J., 2001. Application of Sr isotopes to hydrology of Colorado system waters and potentially related Neogene sedimentary formations. In: Young, R.A., Spamer, E.E. (Eds.), The Colorado River: Origin and evolution: Grand Canyon: Arizona: Grand Canyon Association, Monograph, 12, pp. 167–172.

Phillips, F.M., Hogan, J.F., Mills, S.K., Hendrickx, J.M.H., 2003. Environmental tracers applied to quantifying causes of salinity in arid-region rivers: preliminary results from the Rio Grande, Southwestern USA. In: Alsharhan, A.S., Wood, W.W. (Eds.), Water Resources Perspectives: Evaluation, Management and Policy, 50. Elsevier, New York, pp. 327–334.

Plummer, L.N., Bexfield, L.M., Anderholm, S.K., Sanford, W.E., Busenburg, E., 2004. Geochemical characterization of ground-water flow in the Santa Fe Group aquifer system, Middle Rio Grande Basin, New Mexico. U.S. Geological Survey Water Resources Investigations Report 2003–4131.

Rawling, G.C., Goodwin, L.B., Wilson, J.L., 2001. Internal architecture, permeability structure, and hydrologic significance of contrasting fault-zone types. Geology 29, 43–46.

Rawling, G., Timmons, S., Newton, T., Walsh, P., Land, L., Kludt, T., Timmons, M., Johnson, P., Felix, B., 2008. Sacramento Mountains hydrogeology study. New Mexico Bureau Geological Mines Resources 58 (Open File Report 512).

Reed, M.R., Graham, D.W., 1996. Resolving lithospheric and sub-lithospheric contributions to helium isotope variations in basalts from the southwestern US. Earth and Planetary Science Letters 144, 213–222.

Reiter, M., 2005. Subsurface temperatures and crustal strength changes within the seismogenic layer at arroyo del Coyote in the Socorro seismic area, central Rio Grande Rift, New Mexico. GSA Bulletin 117, 307–318.

Reiter, M., 2009. Heat-flow anomalies crossing New Mexico along La Ristra seismic profile. Lithosphere 1, 88–94.

Reiter, M., Chamberlin, R.M., Love, D.M., 2010. New data reflect on the thermal antiquity of the Socorro magma body locale, Rio Grande Rift, New Mexico. Lithosphere 2, 447–453.

Robinson, D., Scrimgeour, C.M., 1995. The contribution of plant C to soil CO_2 measured using $\delta^{13}C$. Soil Biology and Biochemistry 27, 1653–1656. http://dx.doi.org/10.1016/0038-0717(95)00109-R.

Rowe, E.C., Schilling, J.G., 1979. Fluorine in Iceland and Reykjanes ridge basalts. Nature 279, 33–37.

Roybal, F.E., 1991. Ground-water resources of Socorro County, New Mexico. U.S. Geological Survey Water Resources Investigations Report 89–4083.

Russell, L.R., Snelson, S., 1994. Structure and tectonics of the Albuquerque Basin segment of the Rio Grande rift: insights from reflection seismic data. Geological Society of America Special Paper 291, 83–112.

Rzonca, B., Schulze-Makuch, D., 2003. Correlation between microbiological and chemical parameters of some hydrothermal springs in New Mexico, USA. Journal of Hydrology 280, 272–284.

Sanford, A.R., Mott, R.P., Shuleski, P.J., Rinehart, E.J., Caravella, F.J., Ward, R.M., Wallace, T.C., 1977. Geophysical evidence for a magma body in the vicinity of Socorro, New Mexico. In: Heacock, J.G. (Ed.), The Earth's Crust: Its Nature and Physical Properties: American Geophysical Union Geophysical Monograph, 20, pp. 385–404.

Sano, Y., Marty, B., 1995. Origin of carbon in fumarolic gas from island arcs. Chemical Geology 119, 265–274.

Schilling, J.G., Unni, C.K., Bender, M.L., 1978. Origin of chlorine and bromine in the oceans. Nature 273, 631–636.

Scholle, P., 2003. Geologic map of New Mexico. New Mexico Bureau Geological Mines Resources (Scale 1:500,000).

Sharp, Z., 2007. Principles of Stable Isotope Geochemistry.Prentice Hall, Upper Saddle River, New Jersey (344 pp.).

Sherwood Lollar, B., Ballentine, C.J., O'Nions, R.K., 1997. The fate of mantle-derived carbon in a continental sedimentary basin: integration of C/He relationships and stable isotope signatures. Geochimica et Cosmochimica Acta 61, 2295–2308.

Spiegel, Z., 1955. Geology and ground-water resources of northeastern Socorro County, New Mexico. New Mexico Bureau of Mines and Mineral Resources Ground Water Report 4.

Toth, J., 1963. A theoretical analysis of groundwater flow in small drainage basins. Journal of Geophysical Research 68, 4795–4812.

Trock, W.L., Huszar, P.C., Radosevich, G.E., Skogerboe, G.V., Vlachos, E.C., 1978. Socio-economic and Institutional Factors in Irrigation Return Flow Quality Control Volume III: Middle Rio Grande Valley Case Study.Environmental Protection Agency (Report EPA-600/2-78-174c).

vanDenburgh, A.S., Feth, J.H., 1965. Solute erosion and chloride balance in selected river basins of the western conterminous United States. Water Resources Research 1, 537–541.

Webster, J.D., de Vivo, B., 2002. Experimental and modeled solubilities of chlorine in aluminosilicate melts, consequences of magma evolution, and implications for exsolution of hydrous chloride melt at Mt. Somma-Vesuvius. American Mineralogist 87, 1046–1061.

Welhan, J.A., Poreda, R.J., Rison, W., Craig, H., 1988. Helium isotopes in geothermal and volcanic gases of the western United States, I. Regional variability and magmatic origin. Journal of Volcanology and Geothermal Research 34, 185–199.

Wilcox, L.V., 1957. Analysis of salt balance and salt-burden data on the Rio Grande. In: Duisberg, P.C. (Ed.), Problems of the Upper Rio Grande: An Arid Zone River, 1. U. S. Commission for Arid Resource Improvement and Development, Socorro, New Mexico, pp. 39–44.

Witcher, J.C., King, J.P., Hawley, J.W., Kennedy, J.F., Williams, J., Cleary, M., Bothern, L.R., 2004. Sources of Salinity in the Rio Grande and Mesilla Basin Groundwater.Water Resources Research Institute (Completion Report No. 330).

Woolsey, E.E., Person, M.A., Crossey, L., Phillips, F.M., Karlstrom, K., Williams, A., 2012. Evaluating mantle-to-surface hydrologic connections in the Rio Grande rift using mathematical modeling. Abstract: American Geophysical Union Fall Meeting 2012.

Zhou, Z., Ballentine, C.J., Kipfer, R., Schoell, M., Thibodeaux, S., 2005. Noble gas tracing of groundwater/coalbed methane interaction in the San Juan Basin, USA. Geochimica et Cosmochimica Acta 69, 5413–5428.